Direct interferometric test of the nonlinear phase-shift gate

Peter L. Kaulfuss, Paul M. Alsing, Edwin E. Hach, III, A. Matthew Smith, and Michael L. Fanto

A direct interferometric test of the nonlinear phase shift gate

Peter L. Kaulfuss,[1] Paul M. Alsing,[2, *] Edwin E. Hach III,[1]

A. Matthew Smith,[2] and Michael L. Fanto[2]

[1]*Rochester Institute of Technology, School of Physics and Astronomy,*

85 Lomb Memorial Dr., Rochester, NY 14623

[2]*Air Force Research Laboratory, Information Directorate, 525 Brooks Rd, Rome, NY, 13411*

(Dated: January 6, 2021)

Abstract

Probabilistic quantum gates permeate nearly all aspects of modern linear optical quantum computing. This is largely due to the measurement induced nonlinearities of which they are capable. The trade-off between the cost of resources required to boost success probabilities to scalable levels and the realization effective photon-photon interactions required grows ever-more favorable to this paradigm with rapidly evolving advancements in integrated nano-photonics. As quantum circuits generating cluster states become increasingly complex, component analysis is critical. In this article, we propose and demonstrate the experimental viability of testing a probabilistic gate. Specifically, as an illustrative example of the technique, we propose a direct test of the Non-Linear Phase Shift Gate (NLPSG), an essential component of a Knill Laflamme Milburn Controlled-NOT (KLM CNOT) gate. We develop our analysis for the both the case of the original, bulk optical KLM NLPSG and for the scalable integrated nano-photonic NLPSG based on Micro-Ring Resonators (MRRs) that we have proposed very recently. We consider the interference between the target photon mode of the NLPSG along one arm of a Mach Zehnder Interferometer (MZI) and a mode subject to an adjustable linear phase along the other arm. Analysis of triple-photon coincidences between the two modes at the output of the MZI and the success ancillary mode of the NLPSG provides a signature of the conditionally successful operation of the NLPSG. We examine the triple coincidence results for experimentally realistic cases of click/no-click detection with sub-unity detection efficiencies. Further we compare the case for which the MZI input modes are seeded with weak Coherent States (w-CS) and to that for which the input states are those resulting from colinear Spontaneous Parametric Down Conversion (cl-SPDC). In particular, we show that, though more difficult to prepare, cl-SPDC states offer clear advantages for performing the test, especially in the case of relatively low photon detector efficiency. We develop the interferometric analysis in terms of a general four mode unitary so that comparison and contrast of the signatures of the specific NLPSG implementation (i.e. KLM and MRR) can be carried out easily by substituting in the appropriate unitary matrix elements at the end of the calculation. The analysis is readily extendable to other several mode, low photon number quantum circuits whose success operation is heralded by the measurement of ancilla photons, under non-ideal detection conditions germane to laboratory experiments.

---

* corresponding author: paul.alsing@us.af.mil

I. INTRODUCTION

Probabilistic quantum gates play a central role in modern schemes for photonic quantum information processing [1]. Relatively recent advancements in integrated nanophotonics, especially with respect to the scalability, reproducibility, and packaging of systems, have made the attainment of success probabilities and quantum state fidelities required for the practical deployment of quantum information processing systems ever more feasible due to the accessibility of university and commercial fabrication facilities [2]. It is well-known that direct photon-photon interactions occur only at energy densities far above those achieved in any practical quantum circuit; this makes photons very easy to route through a network using linear optical elements, which, in turn, makes them very appealing as a conduit for quantum information, as evidenced by the very broad interest in schemes involving photonic qubits [3].

The lack of direct, deterministic interaction between photonic qubits does, however, present formidable challenges to the design and optimization of solely photon-based quantum information processing architectures. Ideally, one desires complete optical control of photons in order to implement deterministically multi-qubit quantum gates such as the Controlled-NOT (CNOT) or the Controlled Phase [4]. In the absence of direct, deterministic interactions, one can, in principle, use nonlinear interactions between the photons and an intermediate medium to implement gates. This could be done in a deterministic fashion, if one could identify a material (natural or synthetic) with a large enough nonlinear response. To date, no such material exists. A very recent proposal by Heuck, Jacobs, and Englund seems to represent significant progress toward overcoming the challenge of deterministic, two-qubit processing in the case of the Controlled-Phase Gate [5].

Another approach to the problem involves implementing measurement induced nonlinearities whereby projective measurements on ancillary modes are used to generate an effective nonlinear response in the target modes. This approach is probabilistic owing to the fact that it is a local isometry (i.e. a normalized quantum state vector projection)[6] [7] on the target subsystem that is used to emulate the effect of a nonlinear, deterministic unitary evolution of the same set of target modes. Specifically, conditioned on the results of measurements performed on the ancilla, one can decide whether the desired nonlinear effect in the target has occurred and one can infer the probability with which it does. Perhaps the most famous example of this is the effective bunching of two photons in the signature of the Hong-Ou-Mandel Effect when two photons are coincident on a 50/50 beam-splitter [8, 9]. In the HOM case, measurement of either of the output modes heralds the presence of either, neither, or both photons in the unmeasured mode an effect not attainable

2

classically by any known interaction.

The resource overhead to support the ancillary modes to accommodate the state-reductive transformation required for a probabilistic gate and to provide for the redundancy required to correct for non-unity success probabilities, renders bulk optical implementation of such gates vastly impractical for any practical quantum information processing device. The situation is vastly different with state-of-the art integrated nanophotonic circuits. In fact, the Hong-Ou-Mandel Effect is routinely implemented within the inner workings of a wide variety of quantum photonic circuits [10–14].

Modern paradigms for probabilistic quantum information processing involve the integration of more sophisticated gates, such as fusion gates, in order to reduce the overhead of ancilla required in order to perform a conditional operation, such as CZ, CPHASE, or CNOT with sufficient success probability to be a cost effective quantum resources [10]. The resources required for such systems can be effectively counted in terms of the number of effective KLM CNOT gates required for a given operation to succeed with a given threshold probability [12–14]. The work we present in this paper naturally fits within such a scheme in two distinct ways. First, we present a viable method to perform analysis and tests on basic components of an arbitrary network of the type used for state-of-the-art probabilistic quantum computations. Second, as part of our analysis we keep track of the evolution of both success and failure dynamics of the ancilla within the experimentally viable context of "click/no-click" detection with sub-unity detection efficiencies. Typically, analysis of probabilistic gates performed with state vectors inherently assume unit detection efficiencies and represent the ideal "best-case" operational scenario. By employing non-unit detection efficiencies and an isometry in our analysis we are able to identify and account for the source of "accidental" counts arising from higher photon states that adversely project down into, and contaminates the idealized unit-detection efficiency "signal" that would be observed in an experiment. These two aspects of our work allow for direct feedback for optimizing device design prior to fabrication of integrated photonic processors based on sophisticated architectures such as cluster states and multiplexed fusion gates.

In this paper we propose a direct test that can be applied to the general category of conditional, probabilistic photonic gates that involve a few (illustrated here, 2) ancilla. To demonstrate the analysis, we apply it to the well-known Nonlinear Phase Shift Gate (NLPSG) which belongs within the class of photonic Controlled-Phase gates. The NLPSG is important in its own right owing to its role in the Knill-Laflamme-Milburn Controlled-NOT (KLM CNOT) gate [15, 16]. It is well known that the KLM CNOT has been demonstrated in bulk optics [17]. We are further

motivated here by our recent proposal for a scalable CNOT based upon silicon nanophotonic microring resonators (MRR), which we call an MRR CNOT gate [18]. The direct interferometric test we propose, which is the only one to the best of our knowledge for the NLPSG, relies upon triple-photon coincidence counts in order to expose an effective convolution of the success statistics for the NLPSG with two-photon interference effects in a Mach-Zehnder Interferometer (MZI) [19]. Further, we demonstrate that our direct test is significantly enhanced by the use of output from colinear Spontaneous Parametric Down Conversion (cl-SPDC) in each arm of the MZI [20] . Such a test of the success rate and fidelity of the illustrated gates will be used as design feedback for the integration of scalable circuits such as CNOT [18]. The scalable implementation of any such probabilistic quantum gate opens up the possibility of compact dense circuit integration satisfying engineering redundancy and scaling requirements for practical probabilistic quantum computing [1]. An essential step toward realizing cost effective high yield quantum device fabrication is to develop an approach for component analysis, which we consider to be the essential feature of the work we report in this paper. Strategies related to boosting the success probability of probabilistic-based photonic gates [1] (such as the NLPSG illustrated here) are not addressed in this present work, and will be considered in future works.

The outline of this paper is a follows. In Section II we review the operation of the KLM NLPSG on three modes (one primary mode, and two ancilla modes), and describe our MZI setup for the direct test of the KLM and MRR NLPSG. In Section III we derive the conditions for successful operation of the NLPSG under the action of an arbitrary unitary transformation. Before we embark on the calculation for the coincidence interference probability, we first derive in Section IV the POVM for non-photon number resolving *click/no-click* detection with finite detection efficiencies typical of many laboratory experiments. In Section V we begin our main calculation, and derive the primary interference effect of the coincidence probability using an MZI setup with a NLPSG in one leg and a phase shifter in the other leg. We derive the various interference and accidental output states generated by the even and odd number photon states of weak coherent state (w-CS) inputs, containing up to two photons, in each arm of the MZI. We examine effect of co-linear spontaneous parametric down conversion (cl-SPDC) input states that do not contain the single photon branch, and see that they generate the significant portion of the coincidence interference effect generated by w-CS. Finally, in Section VI we conclude, and discuss the significance of this work for photonic integrated waveguide devices. In the appendices we review the essentials of the KLM and the MRR NLPSG and their maximum success probabilities. Additionally, we remind the reader of the action of a BS on a product of photon Fock states at its inputs ports, which will

be needed for the MZI calculation in Section V. Finally, in the last appendix we explicitly list the coefficients of the four and five photon accidental states that are generated along with the primary coincidence interference effect.

II.   THE NLPSG

As a simple, prototypical quantum circuit relying on (2) ancilla to herald its success probability, we chose the well-known Nonlinear Phase Shift gate (NLPSG) to demonstrate the viability of interferometrically testing a probabilistic quantum gate. The NLSPG has enough simplicity (containing only 4 photon modes) to illustrate the direct interferometric measurement of a non-trivial gate under an isometry and non-unity detection efficiency, while still retaining enough complexity to be of (historical and current) operational interest. The NLPSG was introduced by KLM (Knill, Laflamme and Milburn) [15] in their original proposal for linear optical computing with measurement induced "nonlinearities." In a recent paper [18, 21] we have shown how the original beam splitters (BS) used in the KLM NLPSG could be replaced with micro-ring resonators (which we call the MRR NLPSG) with the net effect of expanding the original point solution space for the optimal success probability to one- and two-dimensional solution manifolds, since the MRR effectively replaces each original BS by two BS and an accumulated MRR phase. In the following, we will first focus on the KLM NLPSG to demonstrate our analysis, but developed in the framework of an arbitrary 4-mode unitary. Afterwards, this will allow us to simply substitute the specific unitary encoding the MRR NLPSG. This analysis is readily adaptable to other moderate photon number unitary gates/circuits. As discussed above, once one employs detectors with non-unit efficiencies, the ideal 3-photon NLPSG success state (resulting from unit detection efficiency) of the NLPSG is insufficient to account for the parasitic accidentals from higher photon states that add to and contaminate the observed signal (e.g. interference pattern). The analysis we develop will then allow allow us to easily compare and contrast the interference signatures of KLM and MRR NLPSG under non-unit detector efficiencies.

We turn our attention first to the KLM NLPSG as a prototypical low (3) photon number quantum gate whose success is heralded by the measurement of (2) ancilla photons. As is widely known, KLM NLPSG [15–18, 21, 22] imparts a phase shift of π on the two-photon branch of any single-mode-1 (normalized) state that evolves through it,

$$|\psi_{(in)}\rangle_{123} = (\alpha_0|0\rangle_1 + \alpha_1|1\rangle_1 + \alpha_2|2\rangle_1) \otimes |1,0\rangle_{2,3},$$
$$\xrightarrow{NLPSG} |\psi_{(out)}\rangle_{123} = (\alpha_0|0\rangle_1 + \alpha_1|1\rangle_1 - \alpha_2|2\rangle_1) \otimes |1,0\rangle_{2,3}, \tag{1}$$

with with $|\alpha_0|^2 + |\alpha_1|^2 + |\alpha_1|^2 = 1$. Typically, this state will be generated as a weak coherent state (w-CS) with mean number of photons $\bar{n}_1 = \alpha^2 \ll 1$, where $\alpha_k = e^{-|\alpha|^2/2} \frac{\alpha^k}{\sqrt{k!}}$. While the input state in mode-1 can be of a general form containing up to two photons, for simplicity we will refer to it in this work as a w-CS. Currently, there is no known way to affect the transformation in Eq.(1) deterministically and nondestructively via unitary evolution. Instead, the transformation is realized probabilistically by using two auxiliary optical modes, here labeled 2 and 3, with one input photon in ancilla mode 2. Projecting out the final state conditioned on a *click* on mode-2 and *no-click* on mode-3 produces the desired local isometry on mode-1 Eq.(1). It has been shown [17, 22] that this action is successful with a maximum probability of $1/4$, and that the result of the projective measurement faithfully indicates the success of the transformation. Consequently, the optimal probability of success for the KLM or MRR CNOT gate is $1/16$ [1,4], which employs two NLPSG. This NLPSG-based CNOT gate effectively performs a HOM [8, 18] interference on the two-photon branch $|2\rangle_1$ of mode-1, in order to affect the CNOT operation on the remaining branch of mode-1, $\alpha_0|0\rangle_1 + \alpha_1|1\rangle_1$.

In this work we consider a direct interferometric coincidence detection of the success probability for both the KLM and MRR implementations of the NLPSG through their insertion into one (upper) leg (mode 1, with ancilla modes 2, 3) of a Mach Zehnder interferometer (MZI) and a PHASE shift element in the other (lower) leg (mode 4), as shown in Fig.(1) [23]. We will consider the case of finite detection efficiencies $\xi_k < 1$ in each mode $1, 2, 3, 4$, which can also can be considered as incorporating propagation and scattering losses. This will allow us to measure the success probability of the NLPSG in the presence of *accidentals*, namely, those coincidence counts that arise from states that are outside the isometry in Eq.(1). These accidentals add a noise floor to the the primary interference effect upon output from the MZI due to the mixing action of the BS and the use of detectors with finite detection efficiencies.

The initial state of the system entering the MZI is

$$|\Psi^{(0)}\rangle = (\alpha_0|0\rangle_1 + \alpha_1|1\rangle_1 + \alpha_2|2\rangle_1) \otimes |1,0\rangle_{2,3} \otimes (\alpha'_0|0\rangle_4 + \alpha'_1|1\rangle_4 + \alpha'_2|2\rangle_4), \quad \sum_{k=0}^2 |\alpha_k|^2 = \sum_{k=0}^2 |\alpha'_k|^2 = 1, \quad (2)$$

with modes $1, 2, 3$ associated with the NLPSG in the upper leg of the MZI and mode 4 in the lower leg (see labeling scheme in Fig.(1)). We can intuitively understand why this state will produce an interference pattern upon coincidence detection of modes 1 and 4 exiting the MZI. The lower leg of the MZI contains a PHASE shift element $e^{i\varphi a_4^\dagger a_4}$ which effectively sends $\alpha'_k \to \alpha'_k e^{ik\varphi}$. Recall that a lossless unitary BS preserves the total photon number entering its ports. Thus, as discussed in detail in Appendix B, a state $|n\rangle_a|m\rangle_b$ entering a BS will generate the $n + m + 1$ states $\{|p\rangle_a|n+m-p\rangle_b\}$
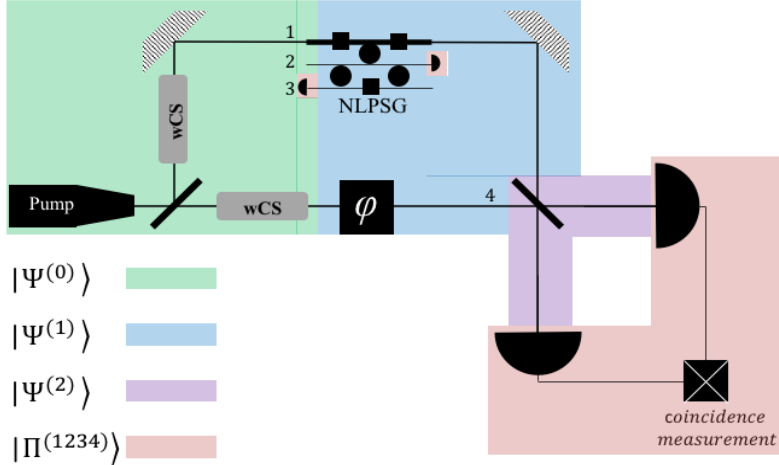
FIG. 1. (Color online) The MRR NLPSG, with the ordinary three beam splitters used in the KLM implementation (see Fig.(4) in Appendix A) replaced by micro-ring resonators (MRRs) (black circles). The input state $|\Psi^{(0)}\rangle$ entering the upper and lower leg of the MZI are weak coherent states (w-CS) of the form $(\alpha_0|0\rangle_1 + \alpha_1|1\rangle_1 + \alpha_2|2\rangle_1)$ and $(\alpha'_0|0\rangle_4 + \alpha'_1|1\rangle_4 + \alpha'_2|2\rangle_4)$, respectively, with the modes of the NLPSG in the upper leg of the MZI labeled (top-down) as $1, 2, 3$. Modes 2 and 3 are the ancilla modes to the NLPSG that are initially in the state $|1, 0\rangle_{2,3}$. The lower leg, mode 4, of the MZI contains a PHASE shift element $e^{i\varphi a_4^\dagger a_4}$ which effectively sends $\alpha'_k \to \alpha'_k e^{ik\varphi}$. The action of $NLPSG_{123} \otimes PHASE_4$ produces the intermediate state $|\Psi^{(1)}\rangle$. The final element of the MZI is a BS of angle θ (such that $\theta = \pi/2$ is a 50:50 BS), whose output is $|\Psi^{(2)}\rangle$. Coincidence detection, producing the un-normalized state $|\tilde{\Psi}^{(2)}\rangle = \Pi^{1234}|\Psi^{(2)}\rangle$, is performed on the exiting modes 1 and 4, conditioned on the NLPSG ancilla modes 2 and 3, occurs with probability $\langle\tilde{\Psi}^{(2)}|\tilde{\Psi}^{(2)}\rangle$. The KLM NLPSG is obtained by replacing each black circle in the NLPSG sub-diagram by a single beam splitter with reflectivities $0 \leq \eta_i \equiv r_i^2 \leq 1$, where and $-1 \leq r_i \leq 1$ are reflection coefficients for $i \in \{1, 2, 3\}$.

where $p \in 0, 1, \ldots, n + m$ with (Wigner) rotation coefficients amplitudes. Thus, upon exit from the MZI, the input states $|0\rangle_1|2\rangle_4$ and $|2\rangle_1|0\rangle_4$ to the final BS will generate the output state $|1\rangle_1|1\rangle_4$ with phase factors proportional to $e^{i\,2\,\varphi}$ and 1 respectively, and BS-dependent modified amplitudes. Similarly, the input state $|1\rangle_1|1\rangle_4$ to the final BS will also generate the output state $|1\rangle_1|1\rangle_4$ with phase factor $e^{i\varphi}$ and a BS-dependent modified amplitude. These two sets of terms, which we will consider individually, contribute to the primary coincidence interference pattern when we condition on the *click*/*no click* of the ancilla modes 2 and 3. Here a *click* detection means that, sans photon number resolving detectors, typical laboratory photon counting experiments are performed with *bucket detectors* (e.g. average efficiency APDs with $\xi_k \simeq 40\%$, or high efficiency SNSPDs with $\xi_k \simeq 85\%$) with the probability to detect n photons scaling as ξ^n. Such higher order detections

are called *accidentals* and contribute an additional noise floor (over that of detector dark counts, which we assume for simplicity to be zero) to the coincidence measurements.

In this work, we will keep track of such accidental terms using the reasonable approximation of detecting at most two photons in any single mode, $1, 2, 3, 4$. We will see that upon output the set of input states $\{|0\rangle_1|2\rangle_4, |2\rangle_1|0\rangle_4\}$ will generate the output state $|1, 1, 0, 1\rangle_{1234} = |1, 1\rangle_{14}|1, 0\rangle_{23}$ upon which the primary interference will be observed, with the output ancilla modes remaining in their ideal "success heralding" state $|1, 0\rangle_{23}$. The output state will also contain (orthogonal) 5-photon states with the the output ancilla modes not necessarily remaining in $|1, 0\rangle_{23}$, plus various other photon Fock states in modes 1 and 4. Similarly, upon output, the input state $|1, 1\rangle_{14}$ will also generate the ideal success state $|1, 1, 0, 1\rangle_{1234}$, as well as 4-photon accidental states. A little forethought indicates that the amplitude of the output state $|1, 1, 0, 1\rangle_{1234}$ will be of the form $(\alpha_0 \alpha_2' A e^{i 2 \varphi} + \alpha_2 \alpha_0' B + \alpha_1 \alpha_1' C e^{i \varphi}) \approx \alpha e^{i \varphi} (A(\theta) e^{i \varphi} + B(\theta) e^{-i \varphi} + C(\theta))$ leading to a primary success probability (squared amplitude) varying as $DC(\theta) + 2 A(\theta) B(\theta) \cos(2 \varphi) + 2 C(\theta) (A(\theta) + B(\theta)) \cos(\varphi)$. Here $A(\theta), B(\theta), C(\theta)$ (taken real for simplicity) will depend on the final BS angle θ, and $DC(\theta) = A(\theta)^2 + B(\theta)^2 + C(\theta)^2$ is the constant (independent of φ) contribution assuming unit detection efficiencies. When finite detection efficiencies are taken into account, there will be a prefactor scaling as $\xi^6 \ll 1$ (assuming, for simplicity, equal detection efficiencies in all modes) as well as both an "$AC(\theta, \phi)$" accidental term (dependent on the phase angle φ, arising from 4-photon output states generated from input states containing $|1\rangle_1$, $|1\rangle_4$, or both) and a $DC(\theta)$ accidental term (arising from the 5-photon states generated by the $|0, 2\rangle_{1,4}$ and $|2, 0\rangle_{1,4}$ input states). Both these accidental states will contribute to the measured coincidence counts. However, these terms will be down in magnitude by factors of $\bar{n} \ll 1$ and $\bar{n}^2 \lll 1$ respectively, from the primary interference probability. The details supporting this intuition will be worked out explicitly in the following sections.

III. THE NLPSG UNDER ARBITRARY UNITARY EVOLUTION

Before we begin the main coincidence measurement calculation, let us first demonstrate the action of the unitary operator U representing the NLPSG on modes 1, 2, 3. Under an arbitrary $N \times N$ unitary evolution U on mode-j, the boson creation operators $a_{in}^\dagger$ are transformed linearly via [22]

$$a_{j,in}^\dagger \rightarrow U a_{j,in}^\dagger U^\dagger = \sum_{k=1}^{N} S_{jk}^T a_{k,out}^\dagger = \sum_{k=1}^{N} a_{k,out}^\dagger S_{kj}, \tag{3}$$

8

where T is transpose, defining the corresponding unitary matrix of coefficients S_{kj} that act as transition coefficients for a photon initially in mode j to be routed to output mode k. Henceforth, we will drop the in, out subscript labels. The action of U on the input state $|\psi_{(in)}\rangle_{123} = (\alpha_0|0\rangle_1 + \alpha_1 |1\rangle_1 + \alpha_2|2\rangle_1) \otimes |1,0\rangle_{2,3}$ of Eq.(1) is then given by [18]

$$|\psi_{(in)}\rangle_{123} = (\alpha_0|0\rangle_1 + \alpha_1 |1\rangle_1 + \alpha_2|2\rangle_1) \otimes |1,0\rangle_{2,3}, \tag{4a}$$
$$= \left(\alpha_0 + \alpha_1 a_1^\dagger + \alpha_2 \frac{a_1^{\dagger 2}}{\sqrt{2}} \right) a_2^\dagger |0,0,0\rangle_{123},$$

$$\xrightarrow{S} |\psi_{(out)}\rangle_{123} = \left[\alpha_0 + \alpha_1 \sum_{j=1}^{3} S_{j1}a_j^\dagger + \alpha_2 \frac{1}{\sqrt{2}} \left(\sum_{j=1}^{3} S_{j1}a_j^\dagger \right) \left(\sum_{k=1}^{3} S_{k1}a_k^\dagger \right) \right] \left(\sum_{\ell=1}^{3} S_{\ell 2}a_\ell^\dagger \right) |0,0,0\rangle_{123},$$
$$\equiv |\psi_{(out)}^{NLPSG}\rangle_{123} + |\psi_{(out)}^\perp\rangle_{123}, \tag{4b}$$

where we have defined the 3-photon NLPSG state $|\psi_{(out)}^{NLPSG}\rangle_{123}$ as

$$|\psi_{(out)}^{NLPSG}\rangle_{123} \equiv \left(\beta_0\, \alpha_0 |0\rangle_1 + \beta_1\, \alpha_1 |1\rangle_1 - \beta_2\, \alpha_2 |2\rangle_1 \right) \otimes |1,0\rangle_{2,3} \tag{5}$$

with the β_k coefficients defined as

$$\text{Condition-0:} \quad \beta_0 = S_{22}, \tag{6a}$$

$$\text{Condition-1:} \quad \beta_1 = S_{11}\, S_{22} + S_{21}\, S_{12}, \tag{6b}$$

$$\text{Condition-2:} \quad \beta_2 = -S_{11}\, (S_{11}\, S_{22} + 2\, S_{21}\, S_{12}), \tag{6c}$$

and

$$|\psi_{out}^\perp\rangle_{123} \equiv \left[\alpha_0 \sum_{\ell \neq 2} S_{\ell 2}a_\ell^\dagger + \alpha_1 \sum_{j,\ell \neq \{(1,2),(2,1)\}} S_{j1}S_{\ell 2}a_j^\dagger a_\ell^\dagger + \frac{1}{\sqrt{2}}\, \alpha_2 \sum_{j,k,\ell \neq \{\text{perm}(1,1,2)\}} S_{j1}S_{k1}S_{\ell 2}\, a_j^\dagger a_k^\dagger a_\ell^\dagger \right] |0,0,0\rangle_{123}, \tag{7}$$

as the remaining "non-NLPSG" state orthogonal to $|\psi_{(out)}^{NLPSG}\rangle_{123}$. Successful operation of the NLPSG occurs when all three conditions Eq.(6a), Eq.(6b), and Eq.(6c) hold simultaneously, namely $\beta_0 = \beta_1 = \beta_2 \equiv \beta$, in which case $|\psi_{(out)}^{NLPSG}\rangle_{123} \rightarrow \beta\, (a_0 |0\rangle_1 + a_1 |1\rangle_1 - \alpha_2 |2\rangle_1$ with success probability $|\beta|^2$. The self consistency of all three conditions requires $S_{11} = 1 \mp \sqrt{2}$, with the physical solution ($|S_{11}| \leq 1$) demanding the solution with the minus sign. The remaining two conditions then demand that

$$P_{\text{success}}^{NLPSG} = |\beta|^2 = |S_{22}|^2 = \frac{1}{2} |S_{21}|^2 |S_{12}|^2, \qquad S_{11} = 1 - \sqrt{2}. \tag{8}$$

This is the operational scenario for the use of two NLPSG in the KLM-CNOT gate [17, 18, 21]. At this stage, the unitary transformation S is arbitrary. In the case of the KLM NLPSG implementation, S is the product of three BS operators. For the MRR NLPSG implementation, as explored in

[18] and discussed in Appendix A, S is the product of three MRR transfer matrix operators. Both these cases will be explored below, but for now we can remain unitarily agnostic, with a general S matrix.

Finally, we note that if one's sole purpose is simply to test the successful sign flip on the state $|2\rangle_1$, (say as an alternative to testing of the validity of the NLPSG with w-CS inputs) then this could also be accomplished by setting $\alpha_1 \equiv 0$, using a co-linear SPDC (cl-SPDC) input state $\alpha_0 |0\rangle_1 + \alpha_2 |2\rangle_1$ and lastly, only requiring that Condition-0 Eq.(6a), and Condition-2 Eq.(6c) hold, namely $\beta_0 = \beta_2 \equiv \beta$, with the value of β_1 unconstrained. While it is easier to generate w-CS than cl-SPDC states, the former which are also more operationally useful in optical quantum computing scenarios, it is informative to also explore the details of the latter case. It will turn out that both types of input states produce nearly identical coincidence interference patterns when the cl-SPDC input state scenario employ detectors operating at 40% detection efficiencies, and the w-CS input state scenario employ detectors with 85% detection efficiencies, both with NLPSG success probabilities of $|\beta|^2 = 1/4$. We will discuss the cl-SPDC scenario in Section V. For now we will explore the case of the general w-CS input state Eq.(4a).

Before we begin the analysis of the MZI interferometer with a NLPSG in one leg and a PHASE shifter in the other, we first examine the POVM operator that is needed to project out the final state (from the MZI-transformed pure input state) that contributes to the coincidence counts.

IV.   *CLICK* AND *NO-CLICK* DETECTION PROJECTION OPERATORS

Since the NLPSG is realized non-deterministically, we first review the concept of non-photon number resolving detection (bucket or *click/no-click* detection) that is typical of many laboratory experiments.

A.   Single mode detection

Consider a detector with probability (detection efficiency) $0 \leq \xi \leq 1$ to detect one photon in a single mode $|1\rangle$, with the corresponding probability $1 - \xi$ not to detect the single photon. Then the projection operators Π_{NC} and Π_C for a *no-click* and a *click* detection, respectively (i.e. non-photon

number resolving detection) are given by

$$\Pi_{NC} = \sum_{n=0}^{\infty} (1 - \xi)^n |n\rangle\langle n| \to |0\rangle\langle 0| \ \text{ as } \ \xi \to 1, \tag{9a}$$

$$\Pi_C = I - \Pi_{NC} = \sum_{n=0}^{\infty} [1 - (1 - \xi)^n] |n\rangle\langle n| \to \sum_{n=1}^{\infty} |n\rangle\langle n| = I - |0\rangle\langle 0| \ \text{ as } \ \xi \to 1, \tag{9b}$$

and hence the pair

$$\text{Single-mode detection POVM} = \{\Pi_C, \Pi_{NC} \equiv I - P_{CC}\}, \tag{10}$$

forms a dichotomous single mode detection POVM. Here, Eq.(9a) is intuitively understood as the probability $(1 - \xi)^n$ not to detect the state $|n\rangle$ of n photons, and for the *no-click* projector Π_{NC} we then sum over all possible photon number states. In the limit of perfect (photon number resolving) detection $\xi \to 1$, we have that Π_{NC} is just the projection onto the vacuum state $|0\rangle\langle 0|$. The opposite case of the detection one or more photons (a *click*) in the given mode is trivially given as $I - \Pi_{NC}$, with the intuitive $\xi \to 1$ limit of $I - |0\rangle\langle 0| = |1\rangle\langle 1| + |2\rangle\langle 2| + \cdots$ (i.e. the projector onto the state containing one or more photons).

The unnormalized state $|\tilde{\Psi}'\rangle$ just after a *click* detection event is given by $|\tilde{\Psi}'\rangle = \Pi_C |\Psi\rangle$ for the pure state $|\Psi\rangle$ just before the measurement. (Note: throughout the paper, we used a *tilde* to indicate an unnormalized state, whose norm yields a probability). The probability for the *click* measurement is then just the norm of this state $P_C = |||\tilde{\Psi}'\rangle||^2 = \langle\Psi|\Pi_C^2|\Psi\rangle$. (Note that while Π_C is a measurement projection operator, it is not a *von-Neumann projection* operator in the sense that $\Pi_C^2 \neq \Pi_C$. Along with Π_{NC}, it is an element of a POVM). This gives the expressions

$$P_{NC} = \text{Tr}[\Pi_{NC} |\Psi\rangle\langle\Psi|] = \sum_{n=0}^{\infty} q_n^2 |\langle n|\Psi\rangle|^2, \qquad q_n = (1 - \xi)^n, \ q_0 = 1, \ q_1 = 1 - \xi, \tag{11a}$$

$$P_C = \text{Tr}[\Pi_C |\Psi\rangle\langle\Psi|] = \sum_{n=0}^{\infty} p_n^2 |\langle n|\Psi\rangle|^2 = 1 - p_{NC}, \ p_n = 1 - q_n, \qquad p_0 = 0, \ p_1 = \xi. \tag{11b}$$

B.   Many mode detection

We can easily extend the concept of *click* and *no-click* detection to many modes. Consider first two modes a and b. If one had *perfect* detection efficiency $\xi \to 1$, the situation in which we *do not* have a simultaneous coincidence click between modes a and b is given by

$$\Pi_{NCC} \underset{\xi \to 1}{\to} |0\rangle_a\langle 0| \otimes I_b + I_a \otimes |0\rangle_b\langle 0| - |0\rangle_a\langle 0| \otimes |0\rangle_b\langle 0|, \tag{12}$$

where the first term is "no-click" in detector A and anything in detector B, the second term is the reverse situation, and the last term with the "-" sign is needed to avoid the double counting of the vacuum projection $|0\rangle_a\langle 0| \otimes |0\rangle_b\langle 0|$ that occurs in the first two terms.

To extend Eq.(12) to imperfect detection $0 \leq \xi_a, \xi_b \leq 1$, we utilize Eq.(9b) to extend $I_a - |0\rangle_a\langle 0| \to \Pi_C^{(a)} = \sum_{n=0}^{\infty} [1 - (1 - \xi_a)^n] |n\rangle_a\langle n| \equiv \sum_{n=0}^{\infty} p_n^{(a)} |n\rangle_a\langle n|$ with $p_n^{(a)} = [1 - (1 - \xi_a)^n]$ the probability *to detect* a "click" of n photons in mode-a Fock state $|n\rangle_a$. Note that $p_0^{(a)} = 0$ and $p_1^{(a)} = \xi_a$. Then, the probability to detect a click in both mode-a and in mode-b, i.e. a *coincidence count* (CC), with finite detection efficiencies is just the *product* of the individual probabilities for mode-a and mode-b, corresponding to the product of the projection operators for each mode, namely

$$\Pi_{CC}^{(ab)} = \Pi_C^{(a)} \otimes \Pi_C^{(b)} = \sum_{n=0}^{\infty} p_n^{(a)} |n\rangle_a\langle n| \otimes \sum_{m=0}^{\infty} p_m^{(b)} |m\rangle_b\langle m|, \tag{13a}$$

$$\equiv \sum_{n=0}^{\infty} \sum_{m=0}^{\infty} p_{nm}^{(ab)} |n,m\rangle_{ab}\langle n,m|, \quad p_{nm}^{(ab)} = [1 - (1 - \xi_a)^n][1 - (1 - \xi_b)^m]. \tag{13b}$$

We see that the above expression has the correct limits, namely $p_{00}^{(ab)} = p_{n0}^{(ab)} = p_{0m}^{(ab)} = 0$ appropriate for *not* detecting a coincidence click, and $p_{11}^{(ab)} = \eta_a \eta_b$. Lastly, the above expression reduces in the limit of unit detection efficiencies to $[I_a - |0\rangle_a\langle 0|] \otimes [I_b - |0\rangle_b\langle 0|]$ such that in the same limit the probability for *no coincidence counts* (NCC) $\Pi_{NCC} = I_a \otimes I_b - \Pi_{CC}$ reduces to the correct limiting form given by Eq.(12). Thus, the dichotomous two-element POVM defining two-mode coincidence *click/no-click* detection is given by

$$\text{Two-mode detection POVM}_{a,b} = \{\Pi_{CC}^{(ab)}, \ \Pi_{NCC}^{(ab)} \equiv I_a \otimes I_b - \Pi_{CC}^{(ab)}\}. \tag{14}$$

This is easily generalized to arbitrary simultaneous coincidence clicks on M modes $a_{i \in \{1,2,...,M\}}$ via

$$M\text{-mode detection POVM}_{a_1,...,a_M} = \{\Pi_{CC}^{(a_1,...,a_M)}, \ P_{NCC}^{(a_1,...,a_M)} \equiv I_{a_1} \otimes ... \otimes I_{a_M} - \Pi_{CC}^{(a_1,...,a_M)}\}, \tag{15a}$$

$$\Pi_{CC}^{(a_1,...,a_M)} = \bigotimes_{i=1}^{M} \Pi_C^{(a_i)}, \quad p_{n_1...n_M}^{(a_1,...,a_M)} = \prod_{i=1}^{M} p_{n_i}^{(a_i)} = \prod_{i=1}^{M} [1 - (1 - \xi_{a_i})^{n_i}]. \tag{15b}$$

The takeaway point of this section is as follows. Under perfect detection efficiency, $\xi_i = 1$ only the state $|1,1,0,1\rangle_{1234}$ will contribute to the probability interference pattern, as discussed in Section II. However, under finite, imperfect detection efficiencies, $\xi_i < 1$, output states other than $|1,1,0,1\rangle_{1234}$ will also contribute to the output detected signal with varying probabilities. We will call such states *accidentals*, since they arise due to finite detection efficiencies. Note that in order to contribute to the total output signal, such states *must* contain at least one photon in each of modes 1, 2, and 4, and any number of photons in mode 3, i.e. $|n_1, n_2, n_3, n_4\rangle_{1234}$ with $n_1, n_2, n_4 \geq 1$, $n_3 \geq 0$.

V. DIRECT MEASUREMENT OF THE NLPSG

In this section we analyze the MZI given in Fig.(1) containing the NLPSG in the upper leg of the MZI, with primary mode 1 and ancilla modes 2 and 3, and the PHASE shift element in the lower leg, mode 4. After the action of $NLPSG_{1,2,3} \otimes PHASE_4$, modes 1 and 4 interfere on a BS_{14}, and are subsequently coincidently detected upon exit from the MZI, while we simultaneously ask for a *click* detection on mode 2 and a *no-click* detection on mode 3. Our unitary operator is given by $\mathcal{U} = BS_{14} \cdot (NLPSG_{123} \otimes PHASE_4)$ and our projection operator will be $\Pi^{(1,2,3,4)} \equiv \Pi_C^{(1)} \otimes \Pi_C^{(2)} \otimes \Pi_{NC}^{(3)} \otimes \Pi_C^{(4)}$. Note that we will explicitly implement (by hand) the phase shift element $PHASE_4 = e^{i \varphi a_4^\dagger a_4}$ on mode 4, which simply has the net effect to transforming $\alpha'_k \rightarrow \alpha'_k e^{i k \varphi}$ on the w-CS$_4$ input state.

A. Preliminaries

As before, we allow the KLM triple BS (or triple MRR) operator on modes $1, 2, 3$ to be represented by S_{ij}, and the BS transformation on modes $1, 4$ to be represented by B_{ij}. Extending these operators to 4×4 matrix representations, we define

$$
\mathcal{B} = \begin{bmatrix} \cos(\theta/2) & 0 & 0 & \sin(\theta/2) \\ 0 & 1 & 0 & 0 \\ 0 & 0 & 1 & 0 \\ -\sin(\theta/2) & 0 & 0 & \cos(\theta/2) \end{bmatrix}, \qquad \mathcal{S} = \begin{bmatrix} S_{11} & S_{12} & S_{13} & 0 \\ S_{21} & S_{22} & S_{23} & 0 \\ S_{31} & S_{32} & S_{32} & 0 \\ 0 & 0 & 0 & 1 \end{bmatrix}, \tag{16}
$$

where the rows and columns are labeled by the mode indices in the order $\{1, 2, 3, 4\}$. (Note, the choice of the argument $\theta/2$ in the BS is so that a 50:50 BS is given by $\theta = \pi/2$). We define the product of these matrices as the unitary $\mathcal{U}$

$$
\mathcal{U} \equiv \mathcal{B}\mathcal{S} = \begin{bmatrix} \cos(\theta/2)\, S_{11} & \cos(\theta/2)\, S_{12} & \cos(\theta/2)\, S_{13} & \sin(\theta/2) \\ S_{21} & S_{22} & S_{23} & 0 \\ S_{31} & S_{32} & S_{32} & 0 \\ -\sin(\theta/2)\, S_{11} & -\sin(\theta/2)\, S_{12} & -\sin(\theta/2)\, S_{13} & \cos(\theta/2) \end{bmatrix}. \tag{17}
$$

The unitary transformation $\mathcal{U}$ affects the following transformations on the boson creation operators

$$
a_i^\dagger \xrightarrow{S} \sum_{j=1}^{4} a_j^\dagger \mathcal{S}_{ji} \xrightarrow{BS} \sum_{j=1}^{4} \sum_{k=1}^{4} a_k^\dagger \mathcal{B}_{kj} \mathcal{S}_{ji} \equiv \sum_{k=1}^{4} a_k^\dagger \mathcal{U}_{ki}, \quad \text{with } \mathcal{U}_{ki} = \sum_{j=1}^{4} \mathcal{B}_{kj} \mathcal{S}_{ji}. \tag{18}
$$

This allows us to transform the initial state $|\Psi^{(0)}\rangle_{1234} \xrightarrow{\mathcal{U}} |\Psi^{(2)}\rangle_{1234}$ (see Fig.(1)). Upon coincidence detection of modes 1 and 4, with *click/no-click* detection on modes 2 and 3, we have the unnormalized post-measurement state $|\Psi^{(1)}\rangle_{1234} \xrightarrow{\Pi^{(1234)}} |\tilde{\Psi}^{(2)}\rangle_{1234}$ (indicated with a *tilde*) with detection probability $P_{1234} = |||\tilde{\Psi}^{(2)}\rangle_{1234}||^2$.

We begin by writing the initial state $|\Psi^{(0)}\rangle_{1234}$, using $\sum_{i=0}^{2} |\alpha_i|^2 = \sum_{i=0}^{2} |\alpha_i'|^2 = 1$ as

$$|\Psi^{(0)}\rangle_{1234} = \left[\alpha_0|0\rangle_1 + a_1|1\rangle_1 + \alpha_2|2\rangle_1\right] \otimes |1,0\rangle_{2,3} \otimes \left[\alpha_0'|0\rangle_4 + \alpha_1'|1\rangle_4 + \alpha_2'|2\rangle_4\right], \tag{19a}$$

$$= \left[\alpha_0\,\alpha_0'\,a_2^\dagger + \alpha_0\,\frac{\alpha_2'}{\sqrt{2}}\,a_2^\dagger\,\left(a_4^\dagger\right)^2 + \frac{\alpha_2}{\sqrt{2}}\,\alpha_0'\,\left(a_1^\dagger\right)^2\,a_2^\dagger + \frac{\alpha_2}{\sqrt{2}}\,\frac{\alpha_2'}{\sqrt{2}}\,\left(a_1^\dagger\right)^2\,a_2^\dagger\,\left(a_4^\dagger\right)^2\right]|0,0,0,0\rangle_{1234} \tag{19b}$$

$$+ \left[\alpha_0\,\alpha_1'\,a_2^\dagger\,a_4^\dagger + \alpha_1\,\alpha_0'\,a_1^\dagger\,a_2^\dagger + \alpha_1\,\alpha_1'\,a_1^\dagger\,a_2^\dagger\,a_4^\dagger + \alpha_1\,\frac{\alpha_2'}{\sqrt{2}}\,a_1^\dagger\,a_2^\dagger\,(a_4^\dagger)^2\right.$$

$$\left. + \frac{\alpha_2}{\sqrt{2}}\,\alpha_1'\,(a_1^\dagger)^2\,a_2^\dagger\,a_4^\dagger\right]|0,0,0,0\rangle_{1234}, \tag{19c}$$

$$\equiv |\Psi^{(0)}_{02';2'0}\rangle + |\Psi^{(0)}_{1,1'}\rangle, \tag{19d}$$

where the input state $|\Psi^{(0)}\rangle_{1234}$ has been separated into two branches. Eq.(19b) separates out that branch $|\Psi^{(0)}_{02';2'0}\rangle$ of the input state that contains only the states $|0\rangle_k$ and $|2\rangle_k$ in modes $k = 1, 4$. Eq.(19c) $|\Psi^{(0)}_{1,1'}\rangle$ separates out the remaining branch of the input state $|\Psi^{(0)}\rangle_{1234}$ that involve either input states $|1\rangle_1$, $|1\rangle_4$, or both.

In the following, we will first concentrate on transformation of the input state $|\Psi^{(0)}_{02';2'0}\rangle$ which after the measurement involves the single 3-photon output state $|1,1,0,1\rangle_{1234}$, and only 5-photon accidental states. Subsequently, we will analyze the transformation of the remaining input state $|\Psi^{(0)}_{1,1'}\rangle$, which after the measurement also involves the output state $|1,1,0,1\rangle_{1234}$, but now with only 4-photon accidental states.

B. Transformation of the input state $|\Psi^{(0)}_{02';2'0}\rangle_{1234}$

After applying the 4×4 unitary $\mathcal{U} = BS_{14} \cdot (NLPSG_{123} \otimes PHASE_4)$ on the mode operators, as illustrated in Fig.(1), we have (note: under $PHASE_4$ we have $|n\rangle_4 \to e^{i\,n\,\varphi}\,|n\rangle_4$ for $n \in \{0,1,2\}$).

$$|\Psi^{(0)}_{0,2';2,0'}\rangle_{1234} \xrightarrow{\text{NLPSG}_{123}\otimes\text{PHASE}_4} |\Psi^{(1)}_{0,2';2,0'}\rangle_{1234} \xrightarrow{BS_{14}} |\Psi^{(2)}_{0,2';2,0'}\rangle_{1234},$$

$$
\begin{aligned}
= \quad & \Bigg[\alpha_0\,\alpha_0'\sum_{j=1}^{4} a_j^\dagger\,\mathcal{U}_{j2} + \alpha_0\,\frac{\alpha_2'}{\sqrt{2}}\,e^{i\,2\,\varphi}\left(\sum_{j=1}^{4} a_j^\dagger\,\mathcal{U}_{j2}\right)\left(\cos(\theta/2)a_4^\dagger + \sin(\theta/2)\,a_1^\dagger\right)^2 \\
+ \quad & \frac{\alpha_2}{\sqrt{2}}\,\alpha_0'\left(\sum_{j=1}^{4} a_j^\dagger\,\mathcal{U}_{j1}\right)\left(\sum_{k=1}^{4} a_k^\dagger\,\mathcal{U}_{k1}\right)\left(\sum_{\ell=1}^{4} a_\ell^\dagger\,\mathcal{U}_{\ell 2}\right) \\
+ \quad & \frac{\alpha_2}{\sqrt{2}}\,\frac{\alpha_2'}{\sqrt{2}}\,e^{i\,2\,\varphi}\left(\sum_{j=1}^{4} a_j^\dagger\,\mathcal{U}_{j1}\right)\left(\sum_{k=1}^{4} a_k^\dagger\,\mathcal{U}_{k1}\right)\left(\sum_{\ell=1}^{4} a_\ell^\dagger\,\mathcal{U}_{\ell 2}\right)\left(\cos(\theta/2)a_4^\dagger + \sin(\theta/2)\,a_1^\dagger\right)^2\Bigg], \quad (20a)
\end{aligned}
$$

$$\xrightarrow{\Pi^{(1234)}} \quad |T_{0,2'}\rangle_{1234} + |T_{2,0'}\rangle_{1234} + |T_{2,2'}\rangle_{1234}. \quad (20b)$$

where in Eq.(20a) we have explicitly carried out the BS transformation on mode-4, $a_4^\dagger \to \cos(\theta/2)\,a_4^\dagger + \sin(\theta/2)\,a_1^\dagger$, (but *not* on mode-1). Additionally, we have explicitly implemented the the PHASE gate $I_{123} \otimes e^{i\,a_4^\dagger a_4\,\varphi}$ on mode-4, which on states sends $|0\rangle_4 \to |0\rangle_4$ and $|2\rangle_4 \to e^{i\,2\,\varphi}\,|2\rangle_4$, and which we have incorporated by hand, having the net effect of sending $\alpha_2' \to \alpha_2'\,e^{i\,2\,\varphi}$. Here the states $|T_{i,j'}\rangle_{1234}$ listed in Eq.(20b), arising from the transformation of the input state $|i\rangle_1\,|j\rangle_4$, are those three or more photon states that survive under measurement projection. Recall that $p_0^{(k)} = 0$ for for mode k, so that the states that remain after projection must contain three or more photons, with at least one photon in each of modes $k = \{1,2,4\}$.

The individual states are given by

$$
\begin{aligned}
|T_{0,2'}\rangle_{1234} &= \alpha_0\,\frac{\alpha_2'}{\sqrt{2}}\,e^{i\,2\,\varphi}\,\sin(\theta)\,\mathcal{U}_{22}|1,1,0,1\rangle_{1234}, \\
&= \alpha_0\,\frac{\alpha_2'}{\sqrt{2}}\,e^{i\,2\,\varphi}\,\sin(\theta)\,S_{22}|1,1,0,1\rangle_{1234}, \quad (21)
\end{aligned}
$$

and

$$
\begin{aligned}
|T_{2,0'}\rangle_{1234} &= \frac{\alpha_2}{\sqrt{2}}\,\alpha_0'\,[\mathcal{U}_{11}\mathcal{U}_{21}\mathcal{U}_{42} + \mathcal{U}_{11}\mathcal{U}_{41}\mathcal{U}_{22} + \mathcal{U}_{21}\mathcal{U}_{11}\mathcal{U}_{42} + \mathcal{U}_{21}\mathcal{U}_{41}\mathcal{U}_{12} + \mathcal{U}_{41}\mathcal{U}_{11}\mathcal{U}_{22} + \mathcal{U}_{41}\mathcal{U}_{21}\mathcal{U}_{12}]\,|1,1,0,1\rangle_{1234}, \\
&= \frac{\alpha_2}{\sqrt{2}}\,\alpha_0'\,\sin(\theta)\,[-S_{11}\,(S_{11}\,S_{22} + S_{21}\,S_{12})]\,|1,1,01\rangle_{1234}, \quad (22)
\end{aligned}
$$

where we recognize β_0 from Eq.(6a) as the amplitude in Eq.(21), and β_2 from Eq.(6c) as the amplitude in Eq.(22). Thus, combining the above two results and upon imposing Condition-0

Eq.(6a) and Condition-2 Eq.(6c) only, which ensures that $\beta_0 = \beta_2 \equiv \beta$, we already have our *primary* interference contribution, namely

$$|T_{0,2'}\rangle_{1234} + |T_{2,0'}\rangle_{1234} = \frac{1}{\sqrt{2}}\sin(\theta)\left[-S_{11}(S_{11}S_{22}+S_{21}S_{12})\alpha_0'\alpha_2+\alpha_0\alpha_2'e^{i\,2\varphi}S_{22}\right]|1,1,0,1\rangle_{1234}, \qquad (23)$$

$$= \frac{1}{\sqrt{2}}\sin(\theta)\,\beta\left[\alpha_0'\alpha_2+\alpha_0\alpha_2'e^{i\,2\varphi}\right]|1,1,0,1\rangle_{1234}, \quad \textit{if impose Conditions 0 \& 2}, \quad (24)$$

$$\to \sqrt{2}\sin(\theta)\,\beta\,|\alpha_0|\,|\alpha_2|\,e^{i\varphi}\cos(\varphi)|1,1,0,1\rangle_{1234}, \quad \text{for } \alpha_0'=\alpha_0 \,\&\, \alpha_2'=\alpha_2. \qquad (25)$$

This last term leads to a coincidence probability arising only from the 3-photon state $|1,1,0,1\rangle_{1234}$ contribution:

$$P_{1234}^{(3-\text{photons})} \to 2\,\xi_1^2\,\xi_2^2\,\xi_4^2\,\sin^2(\theta)\,|\beta|^2\,|\alpha_0|^2\,|\alpha_2|^2\,\cos^2(\varphi), \qquad (26)$$

where we have also included the finite detection efficiency factors.

Lastly, the remaining 5-photon states $|T_{2,2'}\rangle_{1234}$ generated from $\mathcal{U}$ acting on $|\Psi_{0,2';2,0'}^{(0)}\rangle$, which *do not* contribute to the above primary interference pattern are given by

$$\begin{aligned}
|T_{2,2'}\rangle_{1234} = \alpha_2\,\alpha_2'\,e^{i\,2\varphi}\Big(\\
&|1,2,0,2\rangle_{1234}\left[\sin(\theta)\,\mathcal{U}_{202}^{(cs)}+\sin^2(\theta/2)\,\mathcal{U}_{202}^{(ss)}\right]\\
&+|1,2,1,1\rangle_{1234}\left[\sin(\theta)\,\mathcal{U}_{211}^{(cs)}\right]\\
&+|1,1,1,2\rangle_{1234}\left[\sin(\theta)\,\mathcal{U}_{112}^{(cs)}+\sin^2(\theta/2)\,\mathcal{U}_{112}^{(ss)}\right]\\
&+|1,1,2,1\rangle_{1234}\left[\sin(\theta)\,\mathcal{U}_{121}^{(cs)}\right]\\
&+|2,2,0,1\rangle_{1234}\left[\cos^2(\theta/2)\,\mathcal{U}_{201}^{(cc)}+\sin(\theta)\,\mathcal{U}_{201}^{(cs)}\right]\\
&+|2,1,1,1\rangle_{1234}\left[\cos^2(\theta/2)\,\mathcal{U}_{111}^{(cc)}+\sin(\theta)\,\mathcal{U}_{111}^{(cs)}\right]\\
&+|2,1,0,2\rangle_{1234}\left[\cos^2(\theta/2)\,\mathcal{U}_{102}^{(cc)}+\sin(\theta)\,\mathcal{U}_{102}^{(cs)}+\sin^2(\theta/2)\,\mathcal{U}_{102}^{(ss)}\right]\Big), \qquad (27)
\end{aligned}$$

where the various matrix elements $\{\mathcal{U}_{202}^{(cs)},\mathcal{U}_{202}^{(ss)},\ldots\}$ in terms of $\mathcal{U}_{ij}$ are listed explicitly in the Appendix Appendix C. (Note: $\{cc,cs,ss,\}$ superscripts indicate that terms are multiplied by $\{\cos^2(\theta/2),2\cos(\theta/2)\sin(\theta/2),\sin^2(\theta/2)\}$ and $\{c,s\}$ superscripts indicate terms are multiplied by $\{\cos(\theta/2),\sin(\theta/2)\}$. The subscripts i,j,k indicate that the amplitudes multiply the state $|i,j,k\rangle_{2,3,4}$). The important point to note is that by containing 5-photon terms $|T_{2,2'}\rangle_{1234}$ is automatically orthogonal to the 3-photon state $|1,1,0,1\rangle_{1234}$ upon which the primary interference effects occurs. Additionally, each term in Eq.(27) is multiplied by $e^{i\,2\varphi}$, and is also orthogonal to every other term in $|T_{2,2'}\rangle_{1234}$. Hence, upon squaring these amplitudes for the probability, these terms simply contribute to a (BS-angle dependent) dc accidental term $DC(\theta)$, independent of the phase angle φ.

C. Transformation of the input state $|\Psi_{1;1'}^{(0)}\rangle_{1234}$

Turning to the the transformation of the terms listed in Eq.(19c) containing $|1\rangle_1$, $|1\rangle_4$ or both, we have

$$|\Psi_{1,1'}^{(0)}\rangle_{1234} \xrightarrow{\text{NLPSG}_{123}\otimes\text{PHASE}_4} |\Psi_{1,1'}^{(1)}\rangle_{1234} \xrightarrow{BS_{14}} |\Psi_{1,1'}^{(2)}\rangle_{1234},$$

$$= \left[\alpha_0\,\alpha_1' \left(\sum_{j=1}^4 a_j^\dagger\,\mathcal{U}_{j1} \right) \left(\cos(\theta/2)\,a_4^\dagger + \sin(\theta/2)\,a_1^\dagger \right) + \alpha_1\,\alpha_0' \left(\sum_{j=1}^4 a_j^\dagger\,\mathcal{U}_{j1} \right) \left(\sum_{k=1}^4 a_k^\dagger\,\mathcal{U}_{k2} \right) \right.$$

$$+ \alpha_1\,\alpha_1'\,e^{i\,\varphi} \left(\sum_{j=1}^4 a_j^\dagger\,\mathcal{U}_{j1} \right) \left(\sum_{k=1}^4 a_k^\dagger\,\mathcal{U}_{k2} \right) \left(\cos(\theta/2)\,a_4^\dagger + \sin(\theta/2)\,a_1^\dagger \right) \tag{28a}$$

$$+ \alpha_1\,\frac{\alpha_2'}{\sqrt{2}}\,e^{i\,2\,\varphi} \left(\sum_{j=1}^4 a_j^\dagger\,\mathcal{U}_{j1} \right) \left(\sum_{k=1}^4 a_k^\dagger\,\mathcal{U}_{k2} \right) \left(\cos(\theta/2)\,a_4^\dagger + \sin(\theta/2)\,a_1^\dagger \right)^2$$

$$+ \frac{\alpha_2}{\sqrt{2}}\,\alpha_1'\,e^{i\,\varphi} \left(\sum_{j=1}^4 a_j^\dagger\,\mathcal{U}_{j1} \right) \left(\sum_{k=1}^4 a_k^\dagger\,\mathcal{U}_{k1} \right) \left(\sum_{\ell=1}^4 a_\ell^\dagger\,\mathcal{U}_{\ell2} \right) \left(\cos(\theta/2)\,a_4^\dagger + \sin(\theta/2)\,a_1^\dagger \right) \right] |0,0,0,0\rangle_{1234}, \tag{28b}$$

$$\xrightarrow{\Pi^{(1234)}} |T_{1,1'}\rangle_{1234} + |T_{1,2'}\rangle_{1234} + |T_{2,1'}\rangle_{1234}. \tag{28c}$$

Following the same procedure as above, the state that survives after measurement projection and contributes to the primary coincidence interference effect is

$$|T_{1,1'}\rangle_{1234} = \alpha_1\,\alpha_1'\,e^{i\,\varphi}\,|1,1,0,1\rangle_{1234} \left[\cos(\theta/2)\,\mathcal{U}_{101}'^{(c)} + \sin(\theta/2)\,\mathcal{U}_{101}'^{(s)} \right],$$

$$= \alpha_1\,\alpha_1'\,e^{i\,\varphi}\,|1,1,0,1\rangle_{1234}\,\beta_1\cos(\theta), \tag{29}$$

which arises from the transformation of the input state $|1\rangle_1\,|1\rangle_4$. In the above we have defined

$$\beta_1 \equiv S_{11}\,S_{22} + S_{21}\,S_{12} \xrightarrow[\beta\to\beta_{max}=1/2]{} \beta_{max} = 1/2, \quad (\beta_{max}^2 = 1/4), \tag{30}$$

where $\beta_1 \to \beta = 1/2$ *if* we were to impose Condition-1, Eq.(6b) in addition to the previously imposed Condition-0, Eq.(6a) and Condition-2, Eq.(6c), which would then make $\beta^2 \to \beta_{max}^2 = 1/4$.

The remaining 4-photon orthogonal accidental states arising from the transformation of the input states $|1\rangle_1\,|2\rangle_4$ and $|2\rangle_1\,|1\rangle_4$ are given by

$$|T_{1,2'}\rangle_{1234} + |T_{2,1'}\rangle_{1234} =$$

$$\left(e^{i\,\varphi}\,|1,2,0,1\rangle_{1234} \left[\alpha_1\,\alpha_2'\,e^{i\,\varphi}\,\sin(\theta)\,\mathcal{U}_{201}'^{(cs)} + \alpha_2\,\alpha_1' \left(\cos(\theta/2)\,\mathcal{U}_{201}'^{(c)} + \sin(\theta/2)\,\mathcal{U}_{201}'^{(s)} \right) \right] \right.$$

$$+ e^{i\,\varphi}\,|1,1,1,1\rangle_{1234} \left[\alpha_1\,\alpha_2'\,e^{i\,\varphi}\,\sin(\theta)\,\mathcal{U}_{111}'^{(cs)} + \alpha_2\,\alpha_1' \left(\cos(\theta/2)\,\mathcal{U}_{111}'^{(c)} + \sin(\theta/2)\,\mathcal{U}_{111}'^{(s)} \right) \right]$$

$$+ e^{i\,\varphi}\,|1,1,0,2\rangle_{1234} \left[\alpha_1\,\alpha_2'\,e^{i\,\varphi} \left(\sin(\theta)\,\mathcal{U}_{102}'^{(cs)} + \cos^2(\theta/2)\,\mathcal{U}_{102}'^{(cc)} \right) + \alpha_2\,\alpha_1' \left(\cos(\theta/2)\,\mathcal{U}_{102}'^{(c)} + \sin(\theta/2)\,\mathcal{U}_{102}'^{(s)} \right) \right]$$

$$+ e^{i\,\varphi}\,|2,1,0,1\rangle_{1234} \left[\alpha_1\,\alpha_2'\,e^{i\,\varphi} \left(\sin(\theta)\,\mathcal{U}_{101}'^{(cs)} + \sin^2(\theta/2)\,\mathcal{U}_{101}'^{(ss)} \right) + \alpha_2\,\alpha_1' \left(\cos(\theta/2)\,\mathcal{U}_{101}'^{(c)} + \sin(\theta/2)\,\mathcal{U}_{101}'^{(s)} \right) \right] \right), \tag{31}$$

17

Again, the various matrix elements $\{\mathcal{U}_{202}^{\prime(cs)}, \mathcal{U}_{202}^{\prime(ss)}, \ldots\}$ in terms of $\mathcal{U}_{ij}$ are listed explicitly in Appendix C. Note that squaring each of the above amplitudes will generate a $\cos(\varphi)$ higher-order interferences in the accidentals.

D. Form of the unnormalized post measurement state

The complete output state upon transformation by $\mathcal{U}$ for a general w-CS input states on mode 1 and 4 is then

$$|\Psi^{(0)}\rangle_{1234} \xrightarrow{\mathcal{U}} |\Psi^{(2)}\rangle_{1234} \equiv |T_{0,2'}\rangle_{1234} + |T_{2,0'}\rangle_{1234} + |T_{2,2'}\rangle_{1234},$$
$$+ |T_{1,1'}\rangle_{1234} + |T_{1,2'}\rangle_{1234} + |T_{2,1'}\rangle_{1234}. \tag{32}$$

where the top line comes from the transformation of $|\Psi_{02';20}^{(0)}\rangle$ and the bottom line arises from the transformation of $|\Psi_{1,1'}^{(0)}\rangle$. Recall that the state after projection is given by

$$|\tilde{\Psi}^{(2)}\rangle_{1234} \equiv \Pi^{1234} |\Psi^{(2)}\rangle_{1234} = \sum_{n,m,r,s=0}^{4\,\prime} p_n^{(1)} p_m^{(2)} \left(1 - p_r^{(3)}\right) p_s^{(4)} |n,m,r,s\rangle_{1234}\langle n,m,r,s|\Psi^{(2)}\rangle_{1234}, \tag{33}$$

where the prime on the summation indicates that we are in the approximation that each mode contains at most two photons. Since $p_0^{(k)} = 0$, only states with at least one photon in modes $k \in \{1,2,4\}$ survive the measurement projection, and therefore $|\tilde{\Psi}^{(2)}\rangle_{1234}$ contains the 3-photon state $|1,1,0,1\rangle_{1234}$, plus 4- and 5-photon accidental states that also contribute to the coincidence counts when detectors with finite detection efficiencies are employed.

The primary coincidence interference term arises from the $|1,1,0,1\rangle_{1234}$ portion of $|\tilde{\Psi}^{(2)}\rangle_{1234}$ which has the form

$$|\tilde{\Psi}^{(2)}\rangle = (\text{prefactor})^{1/2} \times \left[\beta\, f_3(\theta,\varphi)\, |1,1,0,1\rangle_{1234} + \alpha\, |\tilde{\Psi}_4^{(2)}(\theta,\varphi)\rangle_{1234} + \alpha^2\, |\tilde{\Psi}_5^{(2)}(\theta)\rangle_{1234} \right], \tag{34}$$

where we have defined the prefactor as

$$(\text{prefactor})^{1/2} = \frac{\xi_1\,\xi_2\,\xi_4\,\alpha^2\, e^{i\varphi}}{1 + \alpha^2 + \alpha^4/2} = \frac{\xi_1\,\xi_2\,\xi_4\,\bar{n}\, e^{i\varphi}}{1 + \bar{n} + \bar{n}^2/2}, \tag{35}$$

where $\bar{n} \approx \alpha^2$ is the mean number of photons in the w-CS. Additionally, we define the interference amplitude $f_3(\theta,\varphi)$, after factoring out β, as

Interference Amplitude:

(i) $f_3(\theta,\varphi) = \sin(\theta)\cos(\varphi) + (\beta_1/\beta)\cos(\theta)$, *only assuming* Condition-0 & Condition-2, i.e $\beta_0 = \beta_2 \equiv \beta$, (36)

(ii) $f_3(\theta,\varphi) \to \sin(\theta)\cos(\varphi) + \cos(\theta)$, *additionally* imposing Condition-1, i.e. $\beta_0 = \beta_1 = \beta_2 \equiv \beta$. (37)

Here $|\tilde{\Psi}_4^{(2)}(\theta,\varphi)\rangle_{1234}$ and $|\tilde{\Psi}_5^{(2)}(\theta)\rangle_{1234}$ are (unnormalized state) contributions from the 4-photon and 5-photon states respectively, that contribute to the accidentals, and we have used $\alpha_k' = \alpha_k = \dfrac{\alpha^k}{\sqrt{1 + \alpha^2 + \alpha^4/2}}$ in Eq.(35) for simplicity. θ is the BS angle (with $\theta = \pi/2$ for a 50:50 BS), and φ is the phase shift angle in mode-4. The final interference probability P_{1234}, imposing all three Conditions-0,1,2 then has the form

$$P_{1234} = ||\,|\tilde{\Psi}^{(2)}\rangle_{1234}||^2 = \left[\frac{\xi_1^2\,\xi_2^2\,\xi_4^2\,\bar{n}^2}{(1 + \bar{n} + \bar{n}^2/2)^2}\right]\left[\beta^2\,f_3^2(\theta,\varphi) + \bar{n}\,AC(\theta,\varphi) + \bar{n}^2\,DC(\theta)\right], \quad (38a)$$

$$\bar{n} = \alpha^2, \quad AC(\theta,\varphi) = {}_{1234}\langle\tilde{\Psi}_4^{(2)}|\tilde{\Psi}_4^{(2)}\rangle_{1234} \quad DC(\theta) = {}_{1234}\langle\tilde{\Psi}_5^{(2)}|\tilde{\Psi}_5^{(2)}\rangle_{1234}. \quad (38b)$$

Note that the first and third terms in the right square brackets of Eq.(38a) arise from input states on mode-1 and 4 that contain only 0 and 2 photons when a 50:50 BS ($\theta = \pi/2$) is used (i.e. $\cos(\theta) \to 0$ wipes out the interference contributions arising from the addition of the $|1\rangle_1$ and $|1\rangle_4$ input states). This is of course, just the well known HOM BS-induced interference effect in the context of our NLPSG MZI [8, 24]. Also note that the first (interference) term in Eq.(38a) is of $\mathcal{O}(\beta^2) \sim \mathcal{O}(1)$, while each additional (accidentals) term scales as $\mathcal{O}(\bar{n}) \ll 1$ and $\mathcal{O}(\bar{n}^2) \lll 1$, respectively. Eq.(38a) with Eq.(38b) is one of the main results of this work, to which we will now specialize to both the KLM and MRR implementation of the NLPSG.

In Fig.(2) we plot the scaled probability $P_{1234}'^{(\theta=\pi/2,\varphi)}$ (i.e. defined from Eq.(38a) as $P_{1234} \equiv$ prefactor$\times$ P_{1234}') for coincidences (left) KLM, (right) MRR using co-linear SPDC (cl-SPDC, dashed) and weak coherent (w-CS, solid) input states with a 50:50 BS ($\theta = \pi/2$), and $|\alpha_2/\alpha_0|^2 = 0.1$ with finite detection efficiencies (gray, black) $\xi_1 = \xi_2 = \xi_4 \equiv \xi = \{0.40, 0.85\}$, at the optimal reflection coefficients $r_1^{*2} = r_3^{*2}, r_2^{*2} \Rightarrow |\beta|^2 = 1/4$. The (left) KLM and (right) MRR curves are identical.
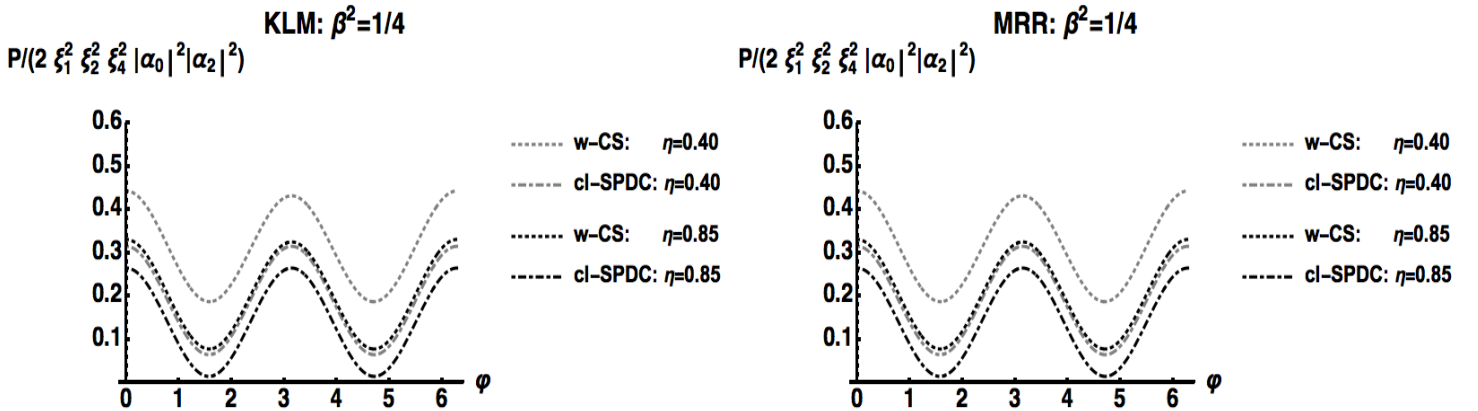

FIG. 2. Plot of P_{1234}' from Eq.(38a) for the (left) KLM, (right) MRR NLPSG for $\beta^2 = 1/4$ for (dotted) w-CS input states and (dot-dashed) cl-SPDC input states with detection efficiencies (gray) 40% and (black) 85%. The left and right graphs are *identical*.

The reason these curves are *identical*, is that even though $S^{(MRR)}$ and $S^{(KLM)}$ are not strictly identical, i.e. $S^{(MRR)} \neq S^{(KLM)}$, they are *effectively identical* in the sense that the upper left 2×2 sub-matrix $\begin{pmatrix} S_{11} & S_{21} \\ S_{21} & S_{22} \end{pmatrix}$, of each unitary matrix are identical at $\beta^2 = 1/4$, which now enforces Condition-1, along with Condition-0 and Condition-2 which were previously satisfied, while the third row and third column of the each unitary matrix are different. This is how the MRR-NLPSG encompasses the KLM-NLPSG (since the former solution was modeled after the latter's). This is *not* the case at other values of $\beta^2 \neq 1/4$.

The new feature using the MRR-NLPSG is the one-dimensional manifold relationship between the *phyisical transmission* coefficients τ_i and $\eta_i = \eta_i(\tau_i)$ of the MRR NLPSG in terms of fictitious KLM *effective refection coefficients* r_i as described in Appendix A, and discussed more fully in [18]. That is, by modeling the solutions of the MRR NLPSG *as if* it were composed of three KLM BS, one finds the MRR solutions for the *fictitious KLM* r_i^* that yield $\beta^2 = 1/4$ define a 1-parameter family (manifold) of *physical MRR transmission* coefficients $\eta_i = \eta_i(\tau_i; r_i^*)$ (this is true *in general* regardless of the value of $r_i \Rightarrow \beta^2$ considered) given by

$$\eta_i(\tau_i; r_i^*) = \frac{r_i^* + \tau_i}{1 + r_i^* \tau_i}, \quad |\tau_i^*| \leq 1 \Rightarrow |\eta_i^*| \leq 1, \quad \text{for fixed} \quad |r_i^*| \leq 1. \quad (39)$$

as shown in Fig.(3). This affords a much greater freedom in the use of the physical transmission
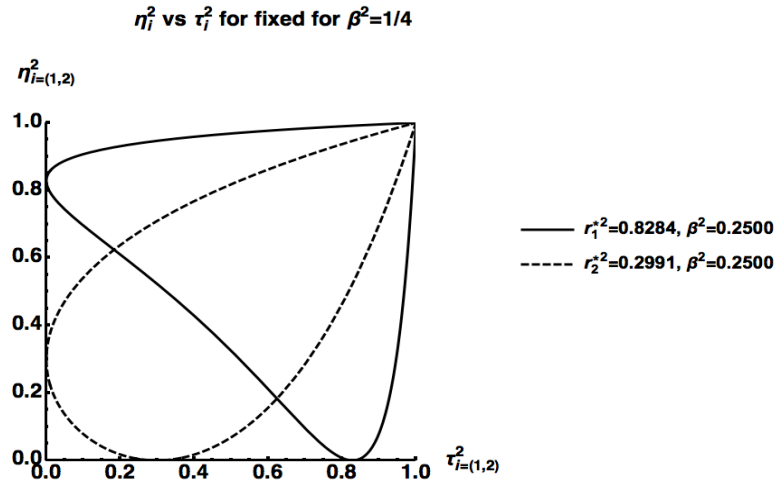

η_i^2 vs τ_i^2 for fixed for $\beta^2 = 1/4$

— $r_1^{*2} = 0.8284, \beta^2 = 0.2500$
---- $r_2^{*2} = 0.2991, \beta^2 = 0.2500$

FIG. 3. Plots of the physical MRR transmissivities (solid) $\eta_{1=3}^2$ vs $\tau_{1=3}^2$, and (dashed) η_2^2 vs τ_2^2 for *fixed* values of the fictitious KLM reflectivities r_1^{*2}, r_2^{*2} yielding $\beta^2 = 1/4$.

coefficients to realize the coincidence interference effect, over the single *point-solution* obtained from the KLM-NLPSG.

All the graphs for a 50:50 BS ($\theta = \pi/2$) have the same qualitative form $P'_{1234} = a_0 + a_1 \cos(\varphi) + \beta^2 \cos^2(\varphi)$ (see Table I). We define the coincidence probability as $P_{1234} = \text{prefactor} \times P'_{1234}$.

Coincidence Detection Probability		
$P'_{1234} = a_0 + a_1 \cos(\varphi) + \beta^2 \cos^2(\varphi)$		
(a_0, a_1) for $\beta^2 = 1/4$		
$\xi \backslash input\ state$	cl-SPDC	w-CS
0.40	(0.065, 0.000)	(0.188, 0.000)
0.85	(0.015, 0.006)	(0.078, 0.003)

TABLE I. Form of the scaled coincidence interference probability $P'_{1234} = a_0 + a_1 \cos(\varphi) + \beta^2 \cos^2(\varphi)$ where the full probability Eq.(38a) is given by $P_{1234} = \text{prefactor} \times P'_{1234}$ (see Table II).

prefactor		
$P_{1234} = \text{prefactor} \times P'_{1234}$		
$\xi \backslash input\ state$	cl-SPDC	w-CS
0.40	6.7×10^{-4}	4.1×10^{-4}
0.85	6.2×10^{-2}	3.8×10^{-2}

Visibilities		
$\beta^2 = 1/4$		
$\xi \backslash input\ state$	cl-SPDC	w-CS
0.40	65%	41%
0.85	89%	65%

TABLE II. (left) prefactor (overall strength of the coincidence interference probability: $P_{1234} = \text{prefactor} \times P'_{1234}$, (right) Visibilities of coincidence interference probability P'_{1234} for input states cl-SPDC and w-CS for $\beta^2 = 1/4$.

Here, the prefactor (see Table II) scales as $\xi^6 \bar{n}^2$ where $\bar{n} = \alpha^2 = \alpha_1^2 = \sqrt{2}\,\alpha_2$ is the mean number of photons in the weak coherent state (w-CS). The upward displacement of the probability curve indicates a larger value of the accidentals - essentially a DC noise offset. In general, the higher the detection efficiency, the lower the noise floor, and the closer the curve nearly touches the abscissa, and consequently, the higher the visibility, as shown in Table II. In both the (left) and (right) figures of Fig.(2) we note that using the cl-SPDC input states at the *lower* detection efficiency of 40% produces nearly the identical curve as using w-CS input states at the much *higher* detection efficiency of 85%.

Note, if we generate input states at a rate r_{states} states/sec and integrate for a time T, then the number of counts is given by $N_{counts} = \text{prefactor} \times r_{states} \times T$ for each of the N_φ discrete values of φ sampled (at minimum 10). This implies that the total time to conduct the experiment will be on the order of $T_{exp} \sim N_\varphi N_{counts}/(\text{prefactor} \times r_{states})$, highlighting the implication of the higher detection efficiency increasing the value of the prefactor, thus reducing T_{exp}. Note that prefactor scales as $\xi_1^2 \xi_2^2 \xi_4^2 \sim \xi^6$ so that a change in detection efficiency from 40% to 85% yields an increase of $(0.85/0.40)^6 = 92 \sim 100X$ in the strength of the effect, while also reducing the strength of the accidentals by $\sim 4X$. The use of more efficient detectors is clearly evident in Table II.

VI. CONCLUSION

In this work we have presented a direct interferometric coincidence test of the KLM- and MRR-based NLPSG for detectors with finite detection efficiencies. The NLPSG was chosen as a prototypical quantum circuit relying on two ancilla to herald its success probability to illustrate the analysis of the direct interferometric testing of low photon number gates expressed as an isometry (i.e. a normalized quantum state vector projection), incorporating non-unit detection efficiencies. In the past, the KLM NLPSG was tested indirectly through the use of two of them to form the basis of a CNOT gate. Essentially, this was a HOM interference on the two-photon branch of the input state (mode 1). Here we propose a straightforward HOM interference setup with a w-CS input state in each arm of a MZI, one arm containing the KLM or MRR NLPSG and the other arm containing a phase shifter. For a 50:50 BS, we show that the primary coincidence interference effect that appears on the ideal NLPSG "success state" arises from the vacuum and two-photon mixing on the final MZI BS, a manifestation of the HOM effect. To make this calculation more experimentally relevant, we keep all terms in the MZI unitary transformation containing up to two photons in each of the four possible modes (three for the NLPSG in one arm of the MZI and one for the phase shifter in the other arm), so that we can include the accidentals that contribute to the coincidence measurement when detectors with finite efficiencies are employed. By developing our analysis in terms of a general 4-mode interaction unitary, we are able to simply substitute the appropriate unitary matrix elements encoding the KLM and the MMR implementation of the NLPSG to compare and contrast their interferometric signatures. With this illustrative quantum circuit we show how the MRR NLPSG encompasses the KLM NLPSG and utilizes the latter's maximum success probability fixed point solution as a parameter in a one dimensional manifold relationship between the physical transmissivities of the each MRR (that now replaces each KLM BS). Lastly, we additionally show that if one instead uses cl-SPDC input states in each arm of the MZI, where the single photon branch is absent, then one obtains qualitatively the same coincidence interference probability, however now with accidentals suppressed by the square of the mean number of photons in the input state, and with a moderately increased interference visibility. While the generation of w-CS is much less resource intensive than that for the production of cl-SPDC states (with corresponding a higher generation rate), both types of inputs states can be utilized to validate the sign-flip by the measurement-induced NLPSG. Both of these approaches could be utilized in current photonic integrated waveguide devices, and experimental verification of these approaches are the focus of follow-on research. The analysis performed in this work, and illustrate with the

22

KLM and MRR NLPSG is readily extendable to other several mode, low photon number quantum circuits whose success operation is heralded by the measurement of ancilla photons, under non-ideal detection conditions germane to laboratory experiments.

[1] M. Gimeno-Segovia, *Towards practical linear optical quantum computing*, https://ethos.bl.uk/OrderDetails.do?uin=uk.bl.ethos.702792 (Department of Physics, Imperial College of London, UK, 2015); S. Morley-Short, *Towards realistic architectures for linear optical quantum computing (Ph.D thesis)*, https://ethos.bl.uk/OrderDetails.do?uin=uk.bl.ethos.774447 (Department of Physics, University of Bristol, UK, 2018).

[2] J. E. Bowers, R. Alferness, R. L. Clark, D. Coolbaugh, L. Kimerling, T. L. Koch, M. Liehr, and M. Watts, *American Institute for Manufacturing Integrated Photonics (AIM Photonics)*, Vol. 2015 IEEE Avionics and Vehicle Fiber-Optics and Photonics Conference (AVFOP) (2015) pp. 24–24.

[3] S. Slussarenko and G. J. Pryde, Appl. Phys. Rev. **66**, 041303 (2019).

[4] P. J. Shadbolt, M. R. Verde, A. Peruzzo, A. Politi, A. Laing, M. Lobinoand, J. C. F. Matthews, M. G. Thompson, and J. L. Obrien, Nature Photonics **6**, 45 (2011).

[5] M. Heuck, K. Jacobs, and D. R. Englund, Phys. Rev. Lett. **124**, 160501 (2020).

[6] An isometry V is a linear map on state vectors between Hilbert spaces $\mathcal{H}$ and $\mathcal{H}'$ of different dimensions. It is a generalization of a unitary transformation and satisfies $VV^{\dagger} = \Pi_{\mathcal{H}'}$ where $\Pi_{\mathcal{H}'}$ is some projection onto $\mathcal{H}'$.

[7] M. M. Wilde, *Quantum Information Theory, 2nd Ed.* (Cambridge University Press, Cambridge, 2017) pp. 144–146.

[8] C. Hong, Z. Ou, and L. Mandel, Phys. Rev. Lett. **59**, 2044 (1987).

[9] C. Gerry and P. L. Knight, *Introductory Quantum Optics* (Cambridge Univeristy Press,Cambridge, 2004).

[10] D. E. Brown and T. Rudolph, Phys. Rev. Letts. **95**, 010501 (2005).

[11] N. S. F. Flamini and F. Sciarrino, Rep. Prog. Phys. **82**, 016001 (2018).

[12] A. M. Childs, D. Maslov, Y. Nam, N. J. Ross, and Y. Sua, PNAS **115**, 9456 (2018).

[13] T. Kim and B. S. Cho, Nature Scientific Reports **8**, 5445 (2018).

[14] J. Abhijith and *et. al.*, arXiv:1804.03719v2 (2020).

[15] E. Knill, R. Laflamme, and G. J. Milburn, Nature **409**, 46 (2001).

[16] K. Kieling, J. Obrien, and J. Eisert, New J. Phys. **12**, 013003 (2010).

[17] R. Okamoto, J. O'brien, H. Hofmann, and S. Takeuchi, PNAS **108**, 10067 (2011).

[18] R. E. Scott, P. M. Alsing, A. M. Smith, M. L. Fanto, C. Tison, and E. E. Hach III, Phys. Rev. A **100**, 022322 (2019).

[19] B. J. Metcalf and *et al.*, Nature Communications **2349**, 1 (2013).

[20] We graciously acknowledge Paul Kwiat for this insightful suggestion conveyed to us at the 1st Photons for Quantum (PfQ) Conference, Rochester Institute of Technology, Rochester, NY, 23-25Jan2019.

[21] P. M. Alsing and E. E. Hach III, Quant. Info Sci. and Tech. IV **10803**, 10803M (2018).

[22] J. Skaar, J. Escartin, and H. Landro, Am. J. Phys. **72**, 1385 (2004).

[23] Though not the primary focus of this work, we note that the schematic shown in Fig.(1) could be implemented in an integrated photonics device as both a NLPSG gate and as a diagnostic interferometric test by replacing the top mirrors with photonic switches (e.g. MZIs or MRRs) so that with the switches *off* the upper leg of the MZI can serve as the circuit throughput signal, while with the switches *on* it can be routed into the 4-mode NLPSG interferometric test.

[24] E. E. Hach III, S. F. Preble, A. W. Elshaari, P. M. Alsing, and M. L. Fanto, Phys. Rev. A **89**, 043805 (2014).

[25] In [18, 21] we labeled the r_i in this work as t_i, and called the later *transmission coefficients*. We followed the calculation of Skaar [22] so that the t_i were in fact actually *reflection* coefficients. All the calculations and conclusions in [18, 21] are uneffected, since the KLM t_i functioned merely as parameters that defined the 1-dimensional manifold relationship between the *physical transmission* coefficients η_i and τ_i of MRR_i, see Eq.(39) and Eq.(A9).

[26] G. S. Agarwal, *Quantum Optics* (Cambridge University Press, Cambridge, 2013).

Appendix A: The KLM and MRR implementation of the NLPSG

1. The KLM NLPSG

The KLM implementation of the NLPSG as shown in Fig.(4) utilized three individual BS of the form
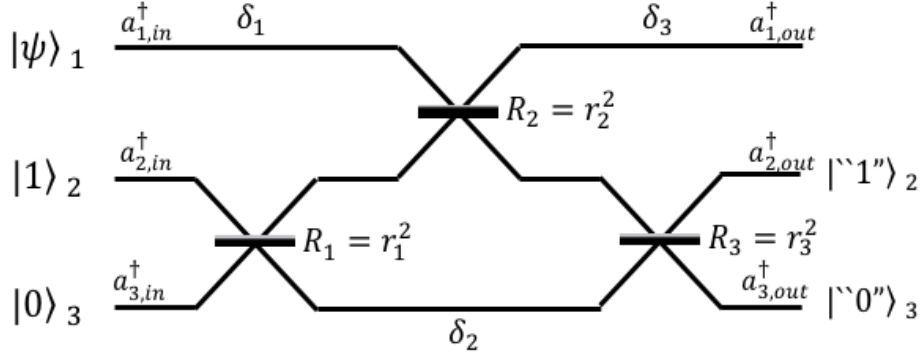

FIG. 4. The KLM NLSG using three ordinary beam splitters of reflectivities $R_i = r_i^2$, and optical path delays of δ_i. Mode 1 is the primary input state in a weak coherent state (w-CS) containing up to two photons. Mode 2 and 3 are ancilla modes, initially in the state $|1,0\rangle_{23}$. Success of NLPSG is heralded by the detection of the output ancilla modes in their initial state.

$$M_1 = \begin{pmatrix} r_1\, e^{i\phi_1} & \sqrt{1-r_1^2} \\ \sqrt{1-r_1^2} & -r_1\, e^{-i\phi_1} \end{pmatrix}, \quad M_2 = \begin{pmatrix} -r_2\, e^{-i\phi_2} & \sqrt{1-r_2^2} \\ \sqrt{1-r_2^2} & r_2\, e^{i\phi_2} \end{pmatrix}, \quad M_3 = \begin{pmatrix} r_3\, e^{i\phi_3} & \sqrt{1-r_3^2} \\ \sqrt{1-r_3^2} & -r_3\, e^{-i\phi_3} \end{pmatrix},$$
$$\tag{A1}$$

with real BS *reflection* coefficients $-1 \le r_i \le 1$ (*reflectivities* $R_i = r_i^2$) [25]. Note that we have chosen a (non-standard) matrix representation of the 2×2 BS matrix that contains only real coefficients [22] such that $\det(M_i) = -1$ for $i \in \{1,2,3\}$.

Recall that a unitary transformation $\mathcal{U} = B_3\, B_2\, B_1$ affects the following transformations on the boson creation operators [18, 21, 22]

$$a_i^\dagger \xrightarrow{B_1} \sum_{j=1}^{4} a_j^\dagger\, (B_1)_{ji} \xrightarrow{B_2} \sum_{j=1}^{4}\sum_{k=1}^{4} a_k^\dagger\, (B_2)_{kj}\, (B_2)_{ji} \xrightarrow{B_3} \sum_{j=1}^{4}\sum_{\ell=1}^{4} a_\ell^\dagger\, (B_3)_{\ell k}\, (B_2)_{kj}\, (B_1)_{ji} \equiv \sum_{k=1}^{4} a_\ell^\dagger\, \mathcal{U}_{\ell i},$$

$$\text{with} \quad \mathcal{U}_{\ell i} = \sum_{k=1}^{4}\sum_{j=1}^{4} (B_3)_{\ell k}\, (B_2)_{kj}\, (B_1)_{ji} \equiv (B_3\, B_2\, B_1)_{\ell i}, \tag{A2}$$

with B_1 acting first, B_2 acting second, and B_3 acting third as we traverse the NLPSG in Fig.(4) from left to right.

Putting the above three blocks together, we have the full evolution from left to right in Fig.(4)

$$\begin{pmatrix} a_{1,out}^\dagger \\ a_{2,out}^\dagger \\ a_{3,out}^\dagger \end{pmatrix}^T = \begin{pmatrix} a_{1,in}^\dagger \\ a_{2,in}^\dagger \\ a_{3,in}^\dagger \end{pmatrix}^T (B_3\,B_2\,B_1) \tag{A3a}$$

$$= \begin{pmatrix} a_{1,in}^\dagger \\ a_{2,in}^\dagger \\ a_{3,in}^\dagger \end{pmatrix}^T \left(\begin{array}{c|cc} e^{i\,\delta_3} & 0 & 0 \\ \hline 0 & & \\ & M_3 \\ 0 & & \end{array} \right) \left(\begin{array}{cc|c} & M_2 & 0 \\ & & 0 \\ \hline 0\ 0 & & e^{i\,\delta_2} \end{array} \right) \left(\begin{array}{c|cc} e^{i\,\delta_1} & 0 & 0 \\ \hline 0 & & \\ & M_1 \\ 0 & & \end{array} \right) \tag{A3b}$$

$$\equiv \begin{pmatrix} a_{1,in}^\dagger \\ a_{2,in}^\dagger \\ a_{2,in}^\dagger \end{pmatrix}^T S \tag{A3c}$$

$$= \begin{pmatrix} a_{1,in}^\dagger \\ a_{2,in}^\dagger \\ a_{3,in}^\dagger \end{pmatrix}^T \begin{pmatrix} S_{11} & S_{12} & S_{13} \\ S_{21} & S_{22} & S_{23} \\ S_{31} & S_{32} & S_{33} \end{pmatrix}, \tag{A3d}$$

where the superscript T indicates the transpose (i.e. the matrix $\mathcal{U} = B_3\,B_2\,B_1$ acts on the row vector $(a_{1,in}^\dagger, a_{2,in}^\dagger, a_{3,in}^\dagger)$ from the right, as in Eq.(A2)). The above product of BS defines the matrix S representing the three mode (1,2,3) KLM NLPSG with components S_{ij} (obtained by explicitly multiplying out $B_3\,B_2\,B_1$) routing a photon initially in mode j (second index) into the mode i (first index). Here, the δ_i represent phase shifts due to the optical path length delays to and from the BSs.

Without loss of generality, we will henceforth only consider the simple case when all phases $\{\phi_i, \delta_i\}$ are identically zero. This yields the S-matrix

$$S^{(KLM)} = \begin{pmatrix} -r_2 & \dfrac{\sqrt{1-r_2^4}}{\sqrt{1+r_2+r_2^2-3\,r_2^3}} & \dfrac{\sqrt{1-r_2^2}\,\sqrt{r_2-3\,r_2^3}}{\sqrt{1+r_2+r_2^2-3\,r_2^3}} \\[1.5em] \dfrac{\sqrt{1-r_2^4}}{\sqrt{1+r_2+r_2^2-3\,r_2^3}} & \dfrac{2\,r_2\,(1+r_2)}{1+2\,r_2+3\,r_2^3} & -\dfrac{\sqrt{1+r_2^2}\,\sqrt{r_2-3\,r_2^3}}{1+2\,r_2+3\,r_2^3} \\[1.5em] \dfrac{\sqrt{1-r_2^2}\,\sqrt{r_2-3\,r_2^3}}{\sqrt{1+r_2+r_2^2-3\,r_2^3}} & -\dfrac{\sqrt{1+r_2^2}\,\sqrt{r_2-3\,r_2^3}}{1+2\,r_2+3\,r_2^3} & \dfrac{1+r_2+r_2^2+3\,r_2^3}{1+2\,r_2+3\,r_2^3} \end{pmatrix}. \tag{A4}$$

Here we have imposed only Condition-0 and Condition-2 so that $\beta_0 = \beta_2 \equiv \beta$ so that

$$r_1(r_2) = r_3(r_2) = \frac{\sqrt{1+r_2^2}}{\sqrt{(1-r_2)\,(1+2\,r_2+3\,r_2^2)}}, \tag{A5a}$$

$$\beta(r_2) = \frac{2\,r_2\,(1+r_2)}{1+2\,r_2+3\,r_2^3} = S_{22}. \tag{A5b}$$

Maximizing β in Eq.(A5b) over r_2 yields the optimal operating values [18, 21, 22]

$$r_2^* = \sqrt{2} - 1 \qquad = 0.424214, \qquad r_2^{*2} = 0.171573, \qquad \text{(A5c)}$$

$$\text{KLM:} \qquad r_1^* = r_3^* = \frac{1}{\sqrt{4 - 2\sqrt{2}}} \quad = 0.92388, \qquad r_1^{*2} = r_3^{*2} = 0.853553, \qquad \text{(A5d)}$$

$$\beta = \frac{1}{2}, \qquad\qquad |\beta|^2 = \frac{1}{4}, \qquad \text{(A5e)}$$

with maximum NLPSG success probability $|\beta|_{max}^2 = 1/4$. Note that due to terms the linear in r_2 in Eq.(A5a) and Eq.(A5b) and $r_1^2(-r_2) \neq r_1^2(r_2)$, we have similarly $|\beta(-r_2)|^2 \neq |\beta(-r_2)|^2$. For example, while $|\beta(-r_2^*)|^2 = 1/2$, we have $r_1^2(-r_2^*) > 1$, and hence this unphysical solution must be rejected.

2. The MRR NLPSG

We now wish to extend the above considerations for the KLM version of the NLPSG to the MRR version [18, 21] by replacing each KLM BS by a MRR. Each MRR_i now has an upper and lower *transmission* coefficient η_i, τ_i, phase angle θ_i, and waveguide bus delays δ_i for $i \in \{1, 2, 3\}$. In [18, 21] the authors modeled the solutions of the MRR NLPSG by treating each MRR element *as if* it had the *form* of a KLM BS with (now complex) *fictitious reflection* coefficients r_i.

The simplest solution was found [18, 21] (mimicking a calculation by Skaar [22]) by considering the case when all the $\theta_i = 0$ (i.e. all MRRs on resonance) and all the bus phase delays were also zero $\delta_i = 0$, so that all the *KLM effective reflection coefficients* r_i were now real. The S matrix for the MRR NLPSG taking $r_3 = r_1$ is given by [18, 21]

$$S^{(MRR)} = \frac{1}{1 - (1 - r_1^2)\, r_2} \begin{pmatrix} (1 - r_1^2) - r_2 & r_1\sqrt{1 - r_2^2} & -r_1\sqrt{1 - r_1^2}\sqrt{1 - r_2^1} \\ r_1\sqrt{1 - r_2^2} & r_1^2\, r_2 & \sqrt{1 - r_1^2}\,(1 - r_2) \\ -r_1\sqrt{1 - r_1^2}\sqrt{1 - r_2^1} & \sqrt{1 - r_1^2}\,(1 - r_2) & r_1^2 \end{pmatrix}.$$

$$\text{(A6)}$$

The form of $S^{(MRR)}$ now differs from that of the KLM case, only because in the MRR case, the middle photon, mode-2 runs *backwards* (right to left), and so there is some involved mode-swap algebra [18, 21] that takes place in forming $S^{(MRR)}$ from $S^{(KLM)}$. As such, it is more compact to write $S^{(MRR)}$ as a function of both r_1 and r_2. Analogous to Eq.(A5a) and Eq.(A5b) we find by imposing only Condition-0 and Condition-2 we have

$$r_1(r_2) = r_3(r_2) = \left[\frac{(1 - r_2)}{r_2\,(1 + r_2^2)} \left((1 + 2\, r_2 - r_2^2) \mp (1 + r_2)\sqrt{(1 - 3\, r_2^2)} \right) \right]^{1/2}, \qquad \text{(A7a)}$$

giving rise to

$$\beta(r_2) = \left(\frac{1}{2 \pm \sqrt{1 - 3\, r_2^2}} \right) \left[\frac{1 + 2\, r_2 - r_2^2}{1 + r_2} \pm \sqrt{1 - 3\, r_2^2} \right], \tag{A7b}$$

where in both Eq.(A7a) and Eq.(A7b) the top sign corresponds to the region $-1/\sqrt{3} \le r_2 \le -1/2$, and the bottom sign to the region $0 \le r_2 \le 1/\sqrt{3}$, which are inequivalent solutions. By additionally imposing Condition-1 and maximizing over r_2 we find analogous to Eq.(A5c)

$$r_2^* = \frac{1 + 2\sqrt{2}}{7} \quad = 0.546918, \qquad r_2^{*2} = 0.299119, \tag{A8a}$$

$$\text{MRR:} \quad r_1^* = r_3^* = \sqrt{2\,(\sqrt{2} - 1)} \quad = 0.91018, \qquad r_1^{*2} = r_3^{*2} = 0.844778, \tag{A8b}$$

$$\beta = \frac{1}{2}, \qquad\qquad\qquad |\beta|^2 = \frac{1}{4}, \tag{A8c}$$

with maximum NLPSG success probability $|\beta|_{max}^2 = 1/4$.

The difference between the analysis in [18, 21] and in this present work is that here we *also* want to consider the case of cl-SPDC input states (only containing the states $|0\rangle_{k \in \{1,4\}}$ and $|2\rangle_{k \in \{1,4\}}$), in addition to the full w-CS input states (also containing the states $|1\rangle_{k \in \{1,4\}}$). In the case of cl-SPDC input states, we will find that *not* imposing Condition-1, namely not letting β_1 to be equal necessarily to β (now defined by imposing *only* Condition-0 and Condition-2) gives qualitatively the same coincidence interference curves. *More importantly*, the MRR solutions for the fictitious KLM reflections coefficients r_i^* define a 1-parameter family of physical *transmission* coefficients $\eta_i = \eta_i(\tau_i; r_i^*)$ regardless of the value of $|\beta|^2$ associated with the chosen value of r_i^*

$$\eta_i(\tau_i; r_i^*) = \frac{r_i^* + \tau_i}{1 + r_i^*\, \tau_i}, \quad |\tau_i| \le 1 \Rightarrow |\eta_i| \le 1, \quad \text{for fixed} \quad |r_i^*| \le 1, \tag{A9}$$

as illustrated in Fig.(5) for values of r_1^{*2} and r_2^{*2} yielding $\beta^2 = 1/4$ for both the KLM-NLPSG and MRR-NLPSG. The analysis for the case of MRR runs similarly for the KLM case by merely replacing $S^{(KLM)} \to S^{(MRR)}$ in the unitary matrix $\mathcal{U}$. The values of r_i^* now differ from the KLM case, only because in the MRR case, the middle photon, mode-2 runs *backwards*, and so there is some mode-swap algebra that takes place in forming $S^{(MRR)}$ from $S^{(KLM)}$.

Appendix B: Action of the BS on $|n, m\rangle_{ab}$

We need to know how an ideal, lossless BS acts on an arbitrary input state $|n, m\rangle$ presented at its two input ports. Let us define the BS transformation (Hamiltonian) on two modes a and b as $BS = (\theta/2)\,(a\, b^\dagger + a^\dagger\, b)$. Here $R \equiv \sin^2(\theta/2)$ is the reflectivity and $T = (1 - R) = \cos^2(\theta/2)$ is the transmissivity, such that $R + T = 1$, as shown in Fig.(6). (Note: we call the quantities $\sin(\theta/2)$
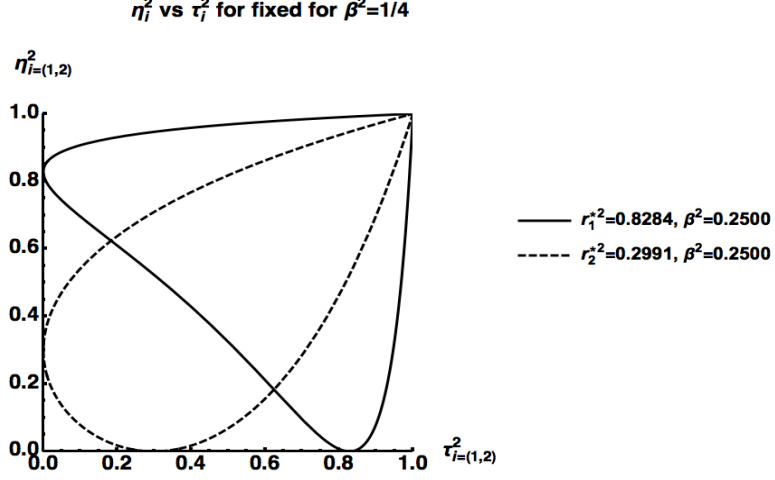
FIG. 5. Plots of the physical MRR transmissivities (solid) $\eta^2_{1=3}$ vs $\tau^2_{1=3}$, and (dashed) η^2_2 vs τ^2_2 for *fixed* values of the fictitious KLM reflectivities r_2^{*2} yielding $\beta^2 = 1/4$. (Fig.(3) repeated here for clarity).

and $\cos(\theta/2)$ reflection and transmission *coefficients*). The factor of $1/2$ in the argument $\theta/2$ is introduced so that $\theta = \pi/2$ represents a 50:50 BS.
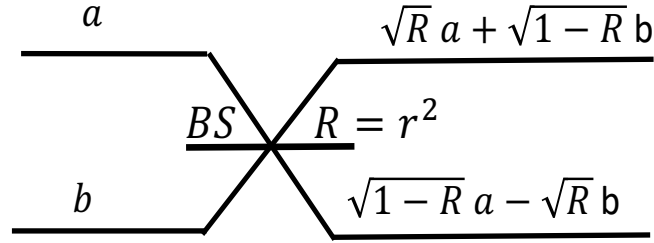

FIG. 6. Two optical modes a and b mixing on a BS of reflectivity R. Note that in this (not always standard) representation the a_{in} mode is the top-left input, while the a_{out} mode is defined via *where a_{in} transmits to,* i.e. as the lower right output. Similarly for b_{in} and b_{out}. Here, the bottom of the BS imparts a π phase shift of -1 upon reflection.

The action of the BS on an arbitrary input of Fock states $|n\rangle_a|m\rangle_b \equiv \dfrac{(a^\dagger)^n}{\sqrt{n!}} \dfrac{(b^\dagger)^n}{\sqrt{m!}} |0\rangle_a|0\rangle_b$ is straightforwardly computed (see Chapter 5 of Agarwal *Quantum Optics* [26]) by applying the BS transformation to the last expression, and expanding out terms using the binomial theorem (since $a^\dagger$ and $b^\dagger$ commute). Note that if we write the BS transformation S_{BS} of the *out* operators in terms of the *in* operators as $\vec{a}^\dagger_{out} = S_{BS}\, \vec{a}^\dagger_{in}$ then to transform an input state such as $|1\rangle_a\,|0\rangle_b = a^\dagger_{in}|0\rangle_a\,|0\rangle_b$, we need to write the *in* operators in terms of the *out* operators using the *transpose* transformation

S_{BS}^T as $\vec{a}_{in}^\dagger = S_{BS}^T \vec{a}_{out}^\dagger$ via

$$\vec{a}_{out}^\dagger = \begin{bmatrix} a_{out}^\dagger \\ b_{out}^\dagger \end{bmatrix} = \begin{bmatrix} \cos(\theta/2) & -\sin(\theta/2) \\ \sin(\theta/2) & \cos(\theta/2) \end{bmatrix} \begin{bmatrix} a_{in}^\dagger \\ b_{in}^\dagger \end{bmatrix} \equiv S_{BS}\, \vec{a}_{in}^\dagger \Rightarrow \vec{a}_{in}^\dagger = S_{BS}^T\, \vec{a}_{out}^\dagger. \quad (B1)$$

Thus, for example $a_{in}^\dagger |0\rangle_a |0\rangle_b \rightarrow \left(\cos(\theta/2)\, a_{out}^\dagger + \sin(\theta/2)\, b_{out}^\dagger \right) |0\rangle_a |0\rangle_b = \cos(\theta/2)\, |1\rangle_a |0\rangle_b + \sin(\theta/2)|0\rangle_a |1\rangle_b$. We can drop all the *in, out* labels and just remember to use the transformation S_{BS}^T in computing the BS transformation formula. The derivation is easily carried out (see also Agarwal [26]) with the results given below using S_{BS}^T to transform an input state $|n\rangle_a |m\rangle_b$ to an output state, yielding

$$|n\rangle_a |m\rangle_b \rightarrow \sum_{p=0}^{n+m} f_p^{(n,m)}\, |p\rangle_a |n+m-p\rangle_b,, \quad (B2)$$

$$f_p^{(n,m)} = \sum_{q=0}^{n} \sum_{q'=0}^{m} \delta_{p,q+q'} \binom{n}{q}\binom{m}{q'} \sqrt{\frac{p!\,(n+m-p)!}{n!\,m!}}\, (-1)^{q'} \left(\cos(\theta/2)\right)^{m+q-q'} \left(\sin(\theta/2)\right)^{n-q+q'}. (B3)$$

Note that the delta function $\delta_{p,q+q'}$ ensures that the BS mixes the original input state $|n\rangle_a |m\rangle_b$ only amongst the $n+m+1$ states of total photon number $n+m$ of the form $\{|0\rangle_a |n+m\rangle_b,\ |1\rangle_a |n+m-1\rangle_b, \ldots |n\rangle_a |m\rangle_b, \ldots, |n+m-1\rangle_a |1\rangle_b,\ |n+m\rangle_a |0\rangle_b\}$. The (real) BS coefficients $f_p^{(n,m)}$ are easily worked out by hand by considering states $|n\rangle_a |m\rangle_b$ up to $n+m=2$ at the input ports of BS, namely:

$$p = 0:$$
$$|0\rangle_a |0\rangle_b \rightarrow |0\rangle_a |0\rangle_b \Rightarrow f_0^{(0,0)} = 1, \quad (B4a)$$
$$p = 1:$$
$$|0\rangle_a |1\rangle_b \rightarrow [\cos(\theta/2)\, b - \sin(\theta/2)\, a]|0\rangle_a |0\rangle_b,$$
$$= \cos(\theta/2)|0\rangle_a |1\rangle_b - \sin(\theta/2)|1\rangle_a |0\rangle_b, \Rightarrow \begin{cases} f_0^{(0,1)} &= \cos(\theta/2) \\ f_1^{(0,1)} &= -\sin(\theta/2) \end{cases} \quad (B4b)$$
$$|1\rangle_a |0\rangle_b \rightarrow [\cos(\theta/2)\, a + \sin(\theta/2)\, b]|0\rangle_a |0\rangle_b,$$
$$= \sin(\theta/2)|0\rangle_a |1\rangle_b + \cos(\theta/2)|1\rangle_a |0\rangle_b, \Rightarrow \begin{cases} f_0^{(1,0)} &= \sin(\theta/2), \\ f_1^{(1,0)} &= \cos(\theta/2), \end{cases} \quad (B4c)$$

$$\quad (B4d)$$

$p = 2$:

$$|0\rangle_a|2\rangle_b = \frac{1}{\sqrt{2}} b^2 |0\rangle_a|0\rangle_b \rightarrow \frac{1}{\sqrt{2}} [\cos(\theta/2)\, b - \sin(\theta/2)\, a]^2 |0\rangle_a|0\rangle_b,$$

$$= \cos^2(\theta/2)|0\rangle_a|2\rangle_b - \sin(\theta)|1\rangle_a|1\rangle_b + \sin^2(\theta/2)|2\rangle_a|0\rangle_b, \Rightarrow \begin{cases} f_0^{(0,2)} = \cos^2(\theta/2), \\ f_1^{(0,2)} = -\frac{1}{\sqrt{2}}\sin(\theta), \quad \text{(B4e)} \\ f_2^{(0,2)} = \sin^2(\theta/2), \end{cases}$$

$$|1\rangle_a|1\rangle_b = a\, b\, |0\rangle_a|0\rangle_b \rightarrow [\cos(\theta/2)\, a + \sin(\theta/2)\, b]\, [\cos(\theta/2)\, b - \sin(\theta/2)\, a]|0\rangle_a|0\rangle_b,$$

$$= \sqrt{2}\, \sin(\theta/2)\, \cos(\theta/2)|0\rangle_a|2\rangle_b[\cos^2(\theta/2) - \sin^2(\theta/2)]|1\rangle_a|1\rangle_b,$$

$$-\sqrt{2}\sin(\theta/2)\, \cos(\theta/2)|2\rangle_a|0\rangle_b, \Rightarrow \begin{cases} f_0^{(1,1)} = \frac{1}{\sqrt{2}}\sin(\theta), \\ f_1^{(1,1)} = \cos(\theta), \quad \text{(B4f)} \\ f_2^{(1,1)} = -\frac{1}{\sqrt{2}}\sin(\theta), \end{cases}$$

$$|2\rangle_a|0\rangle_b = \frac{1}{\sqrt{2}} a^2 |0\rangle_a|0\rangle_b \rightarrow \frac{1}{\sqrt{2}} [\cos(\theta/2)\, a + \sin(\theta/2)\, b]^2 |0\rangle_a|0\rangle_b,$$

$$= \sin^2(\theta/2)|0\rangle_a|2\rangle_b + \sin(\theta)|1\rangle_a|1\rangle_b + \cos^2(\theta/2)|2\rangle_a|0\rangle_b, \Rightarrow \begin{cases} f_0^{(2,0)} = \sin^2(\theta/2), \\ f_1^{(2,0)} = \frac{1}{\sqrt{2}}\sin(\theta), \quad \text{(B4g)} \\ f_2^{(2,0)} = \cos^2(\theta/2), \end{cases}$$

Note: for each (n, m) we have $\sum_{p=0}^{n+m} |f_p^{(n,m)}|^2 = 1$, which just indicates that the BS transformation is unitary. Note that the $f_p^{(n,m)}$ are just the Wigner rotation coefficients for the representation of a system with spin $J = (n+m)/2$ in the angular momentum basis $|J, M\rangle$ with $2J+1 = n+m+1$ states $M \in \{-J, -J+1, \ldots, J\}$ where $M(p) = -J + p\,(2J)/(n+m)$ for $p \in \{0, \ldots, n+m\}$.

Appendix C: $\mathcal{U}$ coefficients for the 4- and 5-photon accidental states

1. The 5-photon accidental states

The 5-photon state $|T_{2,2'}\rangle_{1234}$ in Eq.(20a) proportional to $\alpha_2\, \alpha_2'\, e^{i\,2\,\varphi}$ contributes *accidentals* (noise terms) to the primary coincidence counts by transferring (rerouting) photons *into* states that will be counted as coincidence counts under finite detection efficiencies. These states arise via the BS interaction on mode 1 and 4. These *accidentals* states *do not* contribute to the primary interference terms since they are all part of $|\psi_{out}^\perp\rangle$ and hence are orthogonal to $|1, 1, 0, 1\rangle_{1234}$ upon which the primary coincidence interference effect takes place. Further, since each orthogonal state is multiplied by an *overall* phase factor $e^{i\,2\,\varphi}$, this phase factor squares to unity in the final probability sum, and hence does not even interfere, in higher order, with other states in $|\psi_{out}^\perp\rangle$. Note also that these accidentals involve states with a total photon number of 5, while the primary coincidence

interfering terms contain a total of 3 photons. So our approximation would see a pure coincidence interference pattern if we were to stop at the 3-photon level. However, since our initial input state is already a 5-photon state, a reasonable *self consistent, lowest order* calculation would be to consider states with up to 5 photons, as we do here.

The total number of 5-photon Fock states in $|T_{2,2'}\rangle$ Eq.(20a) is $4^3 \times 3 = 192$ (4 creation operators in each of 3 sums, and 3 terms from expanding the square of the BS operation on mode 4). To get a handle on what terms to keep, it is useful to indicate the possible boson creation operator indices $a_j^\dagger a_k^\dagger a_\ell^\dagger$ as $(j)[k,\ell](1,1)$, $(j)[k,\ell](4,4)$ and $(j)[k,\ell](1,4)$ where the last set of indices in parentheses indicate the terms $(a_1^\dagger)^2$, $(a_4^\dagger)^2$ and $a_1^\dagger a_4^\dagger$ from the expansion of the BS on mode-4. Consider the first set of indices $(1)[k,\ell](11)$. These can be completely eliminated since it contains three 1s corresponding to a state $|3,\cdot,\cdot,\cdot\rangle_{1234}$ which is outside our approximation which keeps terms with at most two photons in any single mode.

For the next set of indices $(2)[k,\ell](11)$ we observe that since there already exists two 1s and one 2, the indices $[k,\ell]$ cannot contain a 1 (since that would give three photons in mode-1), nor can it contain $[k,\ell] = [2,2]$ (since that would give a state with three photons in mode-2). Further, the contributing indices *must* contain as a subset, the indices $\{1,2,4\}$ since terms that don't are multiplied by $p_0^{(1,2,4)} = 0$. Thus the 5 contributing index sets are given by $(2)\{[2,4],[3,4],[4,2],[4,3],[4,4]\}(11)$ corresponding to state $\{|2,2,0,1\rangle_{1234}, |2,1,1,1\rangle_{1234}, |2,2,0,1\rangle_{1234}, |2,1,1,1\rangle_{1234}, |2,1,0,2\rangle_{1234}, \}$, respectively (e.g. $(2)[2,4](11)$ is read off as (11) two photons in mode-1, (22) two photons in mode-2, and (4) one photon in mode-4).

Note that the next set of indices in line $(3)[k,\ell](11)$ only contains two terms $[k,\ell] = \{[2,4],[4,2]\}$ since all dropped terms either do not contain $\{1,2,4\}$, or contains $[k,\ell] = [3,3]$ which yields three photons in mode-3.

Similar to the prior case, the set of contributing indices for $(4)[k,\ell](11)$ are $(4)\{[2,2],[2,3],[2,4],[3,2],[4,2]\}(11)$ corresponding to state $\{|2,2,0,1\rangle_{1234}, |2,1,1,1\rangle_{1234}, |2,1,0,2\rangle_{1234}, |2,1,1,1\rangle_{1234}, |2,1,0,2\rangle_{1234}, \}$, respectively. We can proceed similarly with the $(j)[k,\ell](44)$ and $(j)[k,\ell](14)$, noting right off the bat that we can eliminate the set of indices $(4)[k,\ell](44)$ since it contains three photons in mode-4. The process is an exercise in tedious bookkeeping, but the procedure is straightforward, and yields (note:

32

$\{cc, cs, ss\}$ superscripts indicate terms are multiplied by $\{\cos^2(\theta/2), 2\cos(\theta/2)\sin(\theta/2), \sin^2(\theta/2)\})$

$$|T_{2,2'}\rangle_{1234} = \alpha_2\,\alpha'_2\,e^{i\,2\,\varphi} \times$$

$$|1,2,0,2\rangle_{1234}\left[\sin(\theta)\,\mathcal{U}_{202}^{(cs)} + \sin^2(\theta/2)\,\mathcal{U}_{202}^{(ss)}\right],$$

$$+\,|1,2,1,1\rangle_{1234}\left[\sin(\theta)\,\mathcal{U}_{211}^{(cs)}\right],$$

$$+\,|1,1,1,2\rangle_{1234}\left[\sin(\theta)\,\mathcal{U}_{112}^{(cs)} + \sin^2(\theta/2)\,\mathcal{U}_{112}^{(ss)}\right],$$

$$+\,|1,1,2,1\rangle_{1234}\left[\sin(\theta)\,\mathcal{U}_{121}^{(cs)}\right],$$

$$+\,|2,2,0,1\rangle_{1234}\left[\cos^2(\theta/2)\,\mathcal{U}_{201}^{(cc)} + \sin(\theta)\,\mathcal{U}_{201}^{(cs)}\right],$$

$$+\,|2,1,1,1\rangle_{1234}\left[\cos^2(\theta/2)\,\mathcal{U}_{111}^{(cc)} + \sin(\theta)\,\mathcal{U}_{111}^{(cs)}\right],$$

$$+\,|2,1,0,2\rangle_{1234}\left[\cos^2(\theta/2)\,\mathcal{U}_{102}^{(cc)} + \sin(\theta)\,\mathcal{U}_{102}^{(cs)} + \sin^2(\theta/2)\,\mathcal{U}_{102}^{(ss)}\right], \tag{C1}$$

where we have defined the coefficients of the $|1\rangle_1 \otimes |\cdot,\cdot,\cdot\rangle_{234}$ terms as

$$\mathcal{U}_{202}^{(cs)} = (\mathcal{U}_{21}\,\mathcal{U}_{21}\,\mathcal{U}_{42} + \mathcal{U}_{21}\,\mathcal{U}_{41}\,\mathcal{U}_{22}), \tag{C2a}$$

$$\mathcal{U}_{211}^{(cs)} = \frac{1}{\sqrt{2}}\,(\mathcal{U}_{21}\,\mathcal{U}_{31}\,\mathcal{U}_{22} + \mathcal{U}_{31}\,\mathcal{U}_{21}\,\mathcal{U}_{22}), \tag{C2b}$$

$$\mathcal{U}_{112}^{(cs)} = \frac{1}{\sqrt{2}}\,(\mathcal{U}_{21}\,\mathcal{U}_{31}\,\mathcal{U}_{42} + \mathcal{U}_{21}\,\mathcal{U}_{41}\,\mathcal{U}_{32} + \mathcal{U}_{31}\,\mathcal{U}_{21}\,\mathcal{U}_{42} + \mathcal{U}_{31}\,\mathcal{U}_{41}\,\mathcal{U}_{22} + \mathcal{U}_{41}\,\mathcal{U}_{21}\,\mathcal{U}_{32} + \mathcal{U}_{41}\,\mathcal{U}_{31}\,\mathcal{U}_{22}), \tag{C2c}$$

$$\mathcal{U}_{121}^{(cs)} = \frac{1}{\sqrt{2}}\,(\mathcal{U}_{21}\,\mathcal{U}_{31}\,\mathcal{U}_{32} + \mathcal{U}_{31}\,\mathcal{U}_{21}\,\mathcal{U}_{32} + \mathcal{U}_{31}\,\mathcal{U}_{31}\,\mathcal{U}_{22}), \tag{C2d}$$

$$\mathcal{U}_{112}^{(ss)} = (\mathcal{U}_{11}\,\mathcal{U}_{21}\,\mathcal{U}_{32} + \mathcal{U}_{11}\,\mathcal{U}_{31}\,\mathcal{U}_{22} + \mathcal{U}_{21}\,\mathcal{U}_{11}\,\mathcal{U}_{32} + \mathcal{U}_{21}\,\mathcal{U}_{31}\,\mathcal{U}_{12}), \tag{C2e}$$

$$\mathcal{U}_{202}^{(ss)} = (\mathcal{U}_{31}\,\mathcal{U}_{21}\,\mathcal{U}_{22} + \mathcal{U}_{21}\,\mathcal{U}_{11}\,\mathcal{U}_{22} + \mathcal{U}_{21}\,\mathcal{U}_{21}\,\mathcal{U}_{12}), \tag{C2f}$$

with $\mathcal{U}$ defined from Eq.(17). (Note that the second indices of the triple products of $\mathcal{U}$s are always in the order $\{1,1,2\}$; the first set of indices $\{j,k,\ell\}$ are associated with the state $|j,k,\ell\rangle_{234}$) Similarly, the coefficients of the $|2\rangle_1 \otimes |\cdot,\cdot,\cdot\rangle_{234}$ terms are given by

$$\mathcal{U}_{201}^{(cc)} = (\mathcal{U}_{21}\,\mathcal{U}_{21}\,\mathcal{U}_{24} + \mathcal{U}_{21}\,\mathcal{U}_{41}\,\mathcal{U}_{22} + \mathcal{U}_{41}\,\mathcal{U}_{21}\,\mathcal{U}_{22}), \tag{C3a}$$

$$\mathcal{U}_{111}^{(cc)} = \frac{1}{\sqrt{2}}\,(\mathcal{U}_{21}\,\mathcal{U}_{31}\,\mathcal{U}_{42} + \mathcal{U}_{21}\,\mathcal{U}_{41}\,\mathcal{U}_{32} + \mathcal{U}_{41}\,\mathcal{U}_{31}\,\mathcal{U}_{22}), \tag{C3b}$$

$$\mathcal{U}_{102}^{(cc)} = (\mathcal{U}_{21}\,\mathcal{U}_{41}\,\mathcal{U}_{42} + \mathcal{U}_{41}\,\mathcal{U}_{41}\,\mathcal{U}_{22} + \mathcal{U}_{41}\,\mathcal{U}_{41}\,\mathcal{U}_{22}), \tag{C3c}$$

$$\mathcal{U}_{201}^{(cs)} = (\mathcal{U}_{11}\,\mathcal{U}_{21}\,\mathcal{U}_{22} + \mathcal{U}_{21}\,\mathcal{U}_{11}\,\mathcal{U}_{22} + \mathcal{U}_{21}\,\mathcal{U}_{21}\,\mathcal{U}_{12}), \tag{C3d}$$

$$\mathcal{U}_{111}^{(cs)} = \frac{1}{\sqrt{2}}\,(\mathcal{U}_{11}\,\mathcal{U}_{21}\,\mathcal{U}_{32} + \mathcal{U}_{11}\,\mathcal{U}_{31}\,\mathcal{U}_{22}) + (\mathcal{U}_{21}\,\mathcal{U}_{11}\,\mathcal{U}_{32} + \mathcal{U}_{11}\,\mathcal{U}_{21}\,\mathcal{U}_{32} + \mathcal{U}_{21}\,\mathcal{U}_{31}\,\mathcal{U}_{12}),$$

$$+\,\frac{1}{\sqrt{2}}\,(\mathcal{U}_{31}\,\mathcal{U}_{11}\,\mathcal{U}_{22} + \mathcal{U}_{31}\,\mathcal{U}_{21}\,\mathcal{U}_{12}), \tag{C3e}$$

$$\mathcal{U}_{102}^{(cs)} = (\mathcal{U}_{11}\,\mathcal{U}_{21}\,\mathcal{U}_{42} + \mathcal{U}_{11}\,\mathcal{U}_{41}\,\mathcal{U}_{22} + \mathcal{U}_{21}\,\mathcal{U}_{11}\,\mathcal{U}_{42} + \mathcal{U}_{21}\,\mathcal{U}_{41}\,\mathcal{U}_{12} + \mathcal{U}_{41}\,\mathcal{U}_{11}\,\mathcal{U}_{22} + \mathcal{U}_{41}\,\mathcal{U}_{21}\,\mathcal{U}_{12}), \tag{C3f}$$

$$\mathcal{U}_{102}^{(ss)} = (\mathcal{U}_{11}\,\mathcal{U}_{11}\,\mathcal{U}_{22} + \mathcal{U}_{11}\,\mathcal{U}_{21}\,\mathcal{U}_{12} + \mathcal{U}_{21}\,\mathcal{U}_{11}\,\mathcal{U}_{12}). \tag{C3g}$$

2.   The 4-photon accidental states when $|1\rangle_1$ and $|1\rangle_4$ are included in the input states

Following the same procedure as in the previous section, the coincidence state after projection, will be (note: $\{cc, cs, ss, \}$ superscripts indicate terms are multiplied by $\{\cos^2(\theta/2), 2\,\cos(\theta/2)\sin(\theta/2), \sin^2(\theta/2)\}$ and $\{c, s\}$ superscripts indicate terms are multiplied by $\{\cos(\theta/2), 2\sin(\theta/2)\}$)

$$|T_{1,1'}\rangle_{1234} + |T_{1,2'}\rangle_{1234} + |T_{2,1'}\rangle_{1234} =$$

$$\alpha_1\,\alpha_1'\,e^{i\varphi}\,|1,1,0,1\rangle_{1234}\,\left[\cos(\theta/2)\,\mathcal{U}_{101}'^{(c)} + \sin(\theta/2)\,\mathcal{U}_{101}'^{(s)}\right]$$

$$+e^{i\varphi}\,|1,2,0,1\rangle_{1234}\,\left[\alpha_1\,\alpha_2'\,e^{i\varphi}\,\sin(\theta)\,\mathcal{U}_{201}'^{(cs)} + \alpha_2\,\alpha_1'\,\left(\cos(\theta/2)\,\mathcal{U}_{201}'^{(c)} + \sin(\theta/2)\,\mathcal{U}_{201}'^{(s)}\right)\right],$$

$$+e^{i\varphi}\,|1,1,1,1\rangle_{1234}\,\left[\alpha_1\,\alpha_2'\,e^{i\varphi}\,\sin(\theta)\,\mathcal{U}_{111}'^{(cs)} + \alpha_2\,\alpha_1'\,\left(\cos(\theta/2)\,\mathcal{U}_{111}'^{(c)} + \sin(\theta/2)\,\mathcal{U}_{111}'^{(s)}\right)\right],$$

$$+e^{i\varphi}\,|1,1,0,2\rangle_{1234}\,\left[\alpha_1\,\alpha_2'\,e^{i\varphi}\,\left(\sin(\theta)\,\mathcal{U}_{102}'^{(cs)} + \cos^2(\theta/2)\,\mathcal{U}_{102}'^{(cc)}\right) + \alpha_2\,\alpha_1'\,\left(\cos(\theta/2)\,\mathcal{U}_{102}'^{(c)} + \sin(\theta/2)\,\mathcal{U}_{102}'^{(s)}\right)\right],$$

$$+e^{i\varphi}\,|2,1,0,1\rangle_{1234}\,\left[\alpha_1\,\alpha_2'\,e^{i\varphi}\,\left(\sin(\theta)\,\mathcal{U}_{101}'^{(cs)} + \sin^2(\theta/2)\,\mathcal{U}_{101}'^{(ss)}\right) + \alpha_2\,\alpha_1'\,\left(\cos(\theta/2)\,\mathcal{U}_{101}'^{(c)} + \sin(\theta/2)\,\mathcal{U}_{101}'^{(s)}\right)\right], \quad \text{(C4)}$$

where (Note: all double products $\mathcal{U}\mathcal{U}$ have the second indices in the order $\{1,2\}$, while again all triple products $\mathcal{U}\mathcal{U}\mathcal{U}$ have the second indices in the order $\{1,1,2\}$)

$$\mathcal{U}_{101}'^{(c)} = \mathcal{U}_{11}\mathcal{U}_{22} + \mathcal{U}_{21}\mathcal{U}_{12} = \cos(\theta/2)\,(S_{11}\,S_{22} + S_{21}\,S_{12}) \equiv \cos(\theta/2)\,\beta_1, \qquad\qquad \text{(C5a)}$$

$$\mathcal{U}_{101}'^{(s)} = \mathcal{U}_{21}\mathcal{U}_{42} + \mathcal{U}_{41}\mathcal{U}_{22} = -\sin(\theta/2)\,(S_{21}\,S_{22} + S_{11}\,S_{22}) \equiv -\sin(\theta/2)\,\beta_1, \qquad\qquad \text{(C5b)}$$

$$\mathcal{U}_{201}'^{(cs)} = \mathcal{U}_{21}\mathcal{U}_{22} \qquad\qquad \text{(C5c)}$$

$$\mathcal{U}_{111}'^{(cs)} = \frac{1}{\sqrt{2}}\,(\mathcal{U}_{21}\mathcal{U}_{32} + \mathcal{U}_{31}\mathcal{U}_{22}), \qquad\qquad \text{(C5d)}$$

$$\mathcal{U}_{102}'^{(cs)} = \mathcal{U}_{21}\mathcal{U}_{42} + \mathcal{U}_{41}\mathcal{U}_{22} = -\sin(\theta/2)\,(S_{21}\,S_{12} + S_{11}\,S_{22}) \equiv -\sin(\theta/2)\,\beta_1, \qquad\qquad \text{(C5e)}$$

$$\mathcal{U}_{101}'^{(cs)} = \mathcal{U}_{11}\mathcal{U}_{22} + \mathcal{U}_{21}\mathcal{U}_{12} = \cos(\theta/2)\,(S_{11}\,S_{22} + S_{21}\,S_{12}) \equiv \cos(\theta/2)\,\beta_1, \qquad\qquad \text{(C5f)}$$

$$\mathcal{U}_{102}'^{(cc)} = \mathcal{U}_{11}\mathcal{U}_{22} + \mathcal{U}_{21}\mathcal{U}_{12} = \cos(\theta/2)\,(S_{11}\,S_{22} + S_{21}\,S_{12}) \equiv \cos(\theta/2)\,\beta_1, \qquad\qquad \text{(C5g)}$$

$$\mathcal{U}_{101}'^{(ss)} = \mathcal{U}_{21}\mathcal{U}_{42} + \mathcal{U}_{41}\mathcal{U}_{22} = -\sin(\theta/2)\,(S_{21}\,S_{12} + S_{11}\,S_{22}) \equiv -\sin(\theta/2)\,\beta_1, \qquad\qquad \text{(C5h)}$$

$$\mathcal{U}_{201}'^{(c)} = \mathcal{U}_{11}\mathcal{U}_{21}\mathcal{U}_{22} + \mathcal{U}_{21}\mathcal{U}_{11}\mathcal{U}_{22} + \mathcal{U}_{21}\mathcal{U}_{21}\mathcal{U}_{12}, \qquad\qquad \text{(C5i)}$$

$$\mathcal{U}_{111}'^{(c)} = \frac{1}{\sqrt{2}}\,(\mathcal{U}_{11}\mathcal{U}_{21}\mathcal{U}_{32} + \mathcal{U}_{11}\mathcal{U}_{31}\mathcal{U}_{22} + \mathcal{U}_{21}\mathcal{U}_{11}\mathcal{U}_{32} + \mathcal{U}_{21}\mathcal{U}_{31}\mathcal{U}_{12} + \mathcal{U}_{31}\mathcal{U}_{11}\mathcal{U}_{22} + \mathcal{U}_{31}\mathcal{U}_{21}\mathcal{U}_{12}), \text{(C5j)}$$

$$\mathcal{U}_{102}'^{(c)} = \mathcal{U}_{11}\mathcal{U}_{21}\mathcal{U}_{42} + \mathcal{U}_{11}\mathcal{U}_{41}\mathcal{U}_{22} + \mathcal{U}_{21}\mathcal{U}_{11}\mathcal{U}_{42} + \mathcal{U}_{21}\mathcal{U}_{41}\mathcal{U}_{12} + \mathcal{U}_{41}\mathcal{U}_{11}\mathcal{U}_{22} + \mathcal{U}_{41}\mathcal{U}_{21}\mathcal{U}_{12} \qquad \text{(C5k)}$$

$$\mathcal{U}_{101}'^{(c)} = \mathcal{U}_{11}\mathcal{U}_{11}\mathcal{U}_{22} + \mathcal{U}_{11}\mathcal{U}_{21}\mathcal{U}_{12} + \mathcal{U}_{21}\mathcal{U}_{11}\mathcal{U}_{12}, \qquad\qquad \text{(C5l)}$$

$$\mathcal{U}_{201}'^{(s)} = \mathcal{U}_{21}\mathcal{U}_{21}\mathcal{U}_{42} + \mathcal{U}_{21}\mathcal{U}_{41}\mathcal{U}_{22} + \mathcal{U}_{41}\mathcal{U}_{21}\mathcal{U}_{22}, \qquad\qquad \text{(C5m)}$$

$$\mathcal{U}_{111}'^{(s)} = \frac{1}{\sqrt{2}}\,(\mathcal{U}_{21}\mathcal{U}_{31}\mathcal{U}_{42} + \mathcal{U}_{21}\mathcal{U}_{41}\mathcal{U}_{32} + \mathcal{U}_{31}\mathcal{U}_{21}\mathcal{U}_{42} + \mathcal{U}_{31}\mathcal{U}_{41}\mathcal{U}_{22} + \mathcal{U}_{41}\mathcal{U}_{21}\mathcal{U}_{32} + \mathcal{U}_{41}\mathcal{U}_{31}\mathcal{U}_{22}), \text{(C5n)}$$

$$\mathcal{U}_{102}'^{(s)} = \mathcal{U}_{21}\mathcal{U}_{41}\mathcal{U}_{42} + \mathcal{U}_{41}\mathcal{U}_{21}\mathcal{U}_{42} + \mathcal{U}_{41}\mathcal{U}_{41}\mathcal{U}_{22}, \qquad\qquad \text{(C5o)}$$

$$\mathcal{U}_{101}'^{(s)} = \mathcal{U}_{11}\mathcal{U}_{21}\mathcal{U}_{42} + \mathcal{U}_{11}\mathcal{U}_{41}\mathcal{U}_{22} + \mathcal{U}_{21}\mathcal{U}_{11}\mathcal{U}_{42} + \mathcal{U}_{21}\mathcal{U}_{41}\mathcal{U}_{12} + \mathcal{U}_{41}\mathcal{U}_{11}\mathcal{U}_{22} + \mathcal{U}_{41}\mathcal{U}_{21}\mathcal{U}_{12}. \qquad \text{(C5p)}$$

In the above we have defined as in Eq.(6b)

$$\beta_1 \equiv S_{11} S_{22} + S_{21} S_{12} \xrightarrow[\beta \to \beta_{max}=1/2]{} \beta_{max} = 1/2, \quad (\beta_{max}^2 = 1/4), \tag{C6}$$

where $\beta_1 \to \beta = 1/2$ *if* we were to additionally impose Condition-1 Eq.(6b), which would then make $\beta^2 \to \beta_{max}^2 = 1/4$ when all three Conditions-0,1,2 (Condition-0 Eq.(6a), and Condition-2 Eq.(6c)) are imposed .